NTNU – Trondheim
Norwegian University of
Science and Technology

Carbon Behaviour during Si Production

Zhejun Jin

Silicon and Ferroalloy Production
Submission date: June 2013
Supervisor: Gabriella Tranell, IMTE

Norwegian University of Science and Technology
Department of Materials Science and Engineering

Preface

First and foremost, I would like to express gratitude to my supervisor, Associate Professor Gabriella Tranell, for giving me a great many help during this project and my total Master study.

I would also like to thank Yingda Yu Senior Engineer, who was responsible for my SEM and EDS training; Julian R Tolchard Senior Engineer, who was responsible for my XRD training; Morten Peder Raanes Senior Engineer, who gave me a lot of help during EPMA analysis.

I also appreciate the help from Professor Merete Tangstad, Professor Ragnhild Aune and all the colleagues in our SiManTi Group.

Abstract

The purpose of this work was to research the behaviour of carbon in the process of producing silicon. Carbon material is the main and important raw materials in silicon production because silicon is produced mainly by silica and carbon materials in silicon industry. So the chemical composition and reactivity of carbon material are the crucial properties to the metal yield and purity. In this work, the carbon solubility and behaviour in the silicon or ferrosilicon are also the main issue. In addition, where and how carbide can be formed in the furnace is the focal point.

Prepared samples which were excavated from ferrosilicon furnace were deeper investigated with LOM, XRD, SEM, EDS and EPMA in order to get more information about carbon behaviour such as carbon solubility and trend in different phases.

From this work, I found that the carbon content decreases with the increasing of silicon content in silicon phases. However, the carbon content has no obvious trend in ferrosilicon phases. In addition the carbide can be formed in all locations from the top to the bottom of the ferrosilicon furnace.

List of Abbreviations and Symbols

LOM	Light Optical Microscope
XRD	X-Ray Diffraction
SEM	Scanning Electron Microscope
EDS	Energy Dispersive X-ray Spectrometer
EPMA	Electron Probe Micro Analysis

Contents

1 Introduction

With the development of society and technology, silicon is used in in a large range of applications. It can be used in alloy, electronics, solar cells, and so forth.

Based on purity of the produced silicon, it is generally divided into grades with different applications. Elemental silicon not alloyed with significant quantities of other elements, and usually more than 98%, is often referred to loosely as silicon metal. It makes up about 20% of the world total elemental silicon production, with less than 1 to 2% of total elemental silicon (5–10% of metallurgical grade silicon) ever purified to higher grades for use in electronics. The three most common markets for metallurgical grade silicon are[1]:

1) Alloying of other metals
2) Raw material for the chemical industry
3) Raw material for the semiconductor industry

In the silicon industry, silicon is produced by carbon and silica as main raw materials. So the chemical composition and reactivity of the carbon materials are crucial to the furnace operation and metal yield and purity. The motivation of this project is investigating carbon behaviour and effect during silicon production, in order to improve the silicon process.

The investigation was based on samples from excavated industrial FeSi furnace. And XRD, SEM, EDS and EPMA were used in this project for the research.

The purpose of this work was to research the behaviour of carbon in the process of producing silicon. Carbon material is one of the main raw materials in silicon production. So the chemical composition and reactivity of carbon material are the crucial properties to the metal yield, purity. In this work, the carbon solubility in the silicon or ferrosilicon is also a main issue. In addition, where and how carbide can be

formed in the furnace is the focal point.

2 Background

2.1 Process

In the silicon industry, silicon is produced by carbon and silica as main raw materials. The production processes for ferrosilicon and metallurgical silicon are in principle similar. The main difference in the ferrosilicon process is that iron oxide is added to the furnace. Now the most economically feasible way to produce metallurgical grade silicon is by carbothermic reduction method[2]. A flow sheet of silicon production plant is shown in Figure 2.1. Quartz, iron ore and carbon materials are added to an electric arc furnace. The different of mixture between these reactants depends on the content of silicon in the ferro alloyed product.

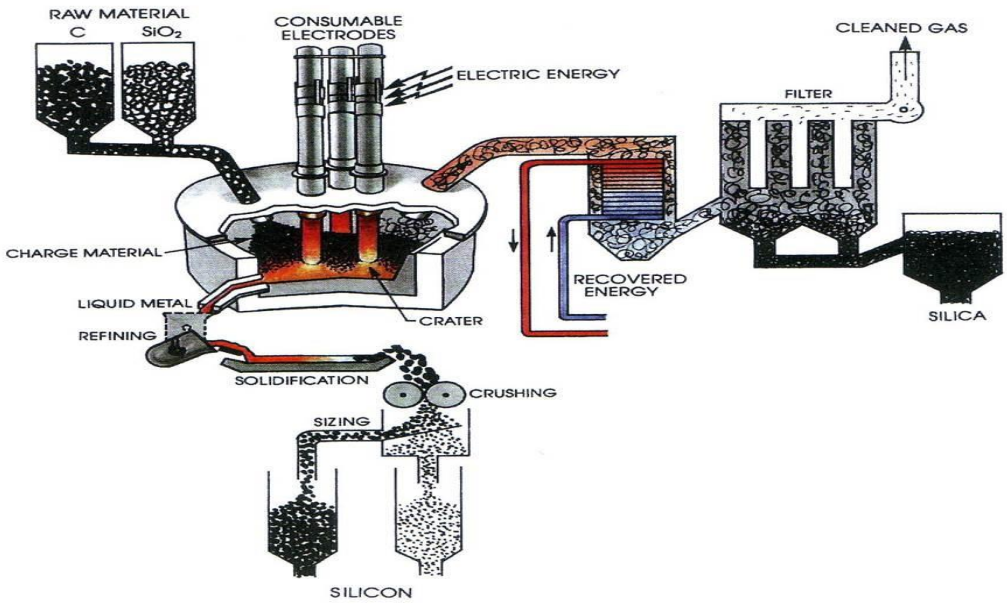

Figure 2.1 A typical plant for production of silicon metal[1].

A typical diameter for silicon furnace is 10m. There are three electrodes submerged into the charge. They supply a three phase current that passes through the charge of the furnace and the productions demands 11-13MWh/ton produced silicon metal. And

the furnace is rotating in a very slow mode that could be from 10 to 40 days. There are some furnaces that are rotating in an oscillating movement, the furnace rotates for as sample clockwise 180^{o} and returns counter clockwise at starting point. The furnace consists of hood at the upper part of furnace that directs the hot gases to a chimney that transport these to a gas cleaning system[1]. The material quartz/quartzite, iron ore, coke/coal and wood chips are mixed through charging tubes. These tubes are located with outlets towards the electrodes. The numbers of tubes surrounding the electrodes differs from furnace to furnace[3]. The liquid alloy product is tapped from a tap hole in the furnace lining. The number of tap holes differs from furnace to furnace and the tap holes can be opened either mechanically or chemically. The tap hole is closed with a specific clay mixture. The melt is tapped from the furnace into a steel ladle which interior is protected with a high temperature resistant refractory material and subsequently cask into specific steel moulds. The cast material is removed from the mould when it has cooled down to a level where the material strength is high enough to be removed and stacked in piles for further cooling[1]. The final product is manufactured depending on the demands by crushing, sieving and granulating.

The off gases are filtered to extract a dust containing mainly amorphous condensed SiO_2 which can be used in concrete, ceramics, refractory and other suitable applications. A furnace produces 0.2-0.4 tons of silica per ton of silicon metal. The filtered off gases are mainly includes SO_2, CO_2, CO and NO_x. The waste heat from the furnace can be used as energy to produce electricity or for some other general heating purposes.

This process flow sheet is almost same as a ferrosilicon production plant where iron-containing raw material is added to the furnace which is under similar conditions as the metallurgical silicon furnace. The main iron-containing raw material is iron oxide which is in the form of pelletised hematite. The hematite is reduced with carbon materials such as coke, coal and wood chips. The content of silicon in the ferrosilicon product differs depending on the requirement.

2.2 Raw materials

As already mentioned above, quartz, pelletised hematite, coke/coal and wood chips.

The wood chips in this production are not only used as reductant but also to improve permeability of the charged material to achieve good gas flow. The wood chips go through pyrolysis where carbonisation happens at higher temperatures to form charcoal[1].

Higher need for purity prefers the use of quartz than quartzite in silicon production. The quartz raw material contains impurities such as Al, Ca, Fe, B, P and Ti. Size of material differs from plant to plant but 10-150 mm is a general size requirement. Quartz is the mineral form of SiO_2. It occurs in igneous, sedimentary, metamorphic and hydrothermal mineral environments. It is generally colourless but different variable colours have been described as pink, purple (amethyst), yellow (citrine) and smoky quartz[2]. The stable polymorphs as atmospheric pressure at different temperature are α-quartz, β-quartz, HL-tridymite and β-cristobalite[4]. In environmental aspects, very fine dust from quartzite may cause health problems for workers if inhaled. Silicosis which is a lung disease, is caused by long term inhalation of quartzite dust. Now, this problem has been solved in modern automized plants[1].

Carbon materials are the main reduction materials in silicon production and the quality of carbon materials is very essential to achieve high silicon yields. Carbon raw materials are generally from coal, charcoal, coke and woodchips. In these four types of carbon materials, the silicon production favors coal and charcoal because they have higher fix-C than the others. Coal also has lower electrical resistivity than other three types of carbon materials[1]. Consequently, coal has better effect on increasing carbon reactivity and reducing energy consumption in silicon furnace. Coal is structurally a complex system where organic material is the dominating species. These organic materials occur in various different petrographic types called macerals. Various amount if inorganic materials are also present in the coal. The structure of coal is an extensive network of pores which gives coal a high surface area[1, 5].

Silicon is the second most abundant element making up 25.7% of the Earth's crust by mass. Silicon is a grey metallic looking crystalline solid. It is not classified as a metal but a metalloid because of its low electrical conductivity. The element crystallizes in the same pattern as a diamond in two inter-penetrating face centred cubic[3, 6].

One of the intermediate reaction products is SiC. The most commonly encountered silicon carbide formed above 2000^{o}C is alpha silicon carbide (α-SiC) that has a hexagonal crystal structure which is similar to Wustite. Another common structure is beta silicon carbide (β-SiC) which has similar structure as zinc blende and it is formed at temperatures below 2000^{o}C. SiC is impossible to grow single crystal in the stoichiometric liquid because it is a covalent compound without congruent melting point[3, 7].

Metallic iron as scrap or iron oxide ore is used as iron source for making ferrosilicon. The main iron-containing raw material is iron oxide which is in the form of pelletised hematite (Fe_2O_3). The pellet is an agglomerated sintered product with a size from 8 to 12 mm. The most common phases of ferrosilicon are FeSi (Fersilite), $FeSi_2$ (Ferdisilite) and Fe_3Si (Suessite)[3, 4].

2.3 Theory

2.3.1 The Si-O-C system

The silicon production can be shown with the reaction (2.1). However, the reactions in the furnace are complex and there are a lot of different side reactions because of the different temperature zones inside the furnace. A high content of SiO gas would be involved in the gas in the hottest temperature zone. So the SiO gas has to be recovered in order to achieve a high silicon recovery. The recovering reaction happens in the outer charge layer where it can heat the charge to a high temperature. The off-gas from the furnace will also contain silicon dioxide, which can be used in a micro silicon plant. The liquid silicon is produced by several intermediate reactions.

SiO_2 (s) + 2C (s) = Si (l) + 2CO (g) (2.1)

In order to better understand, Gibbs phase rule can be used to determine the Si-O-C system with equation (2.2).

P + F = C + 2 (2.2)

The number of components C is three which has several different combinations. P is the number of phases is always present in the reduction process of silicon. It is an invariant system with four condensed phases and a gas phase. The four known condensed phases are silicon dioxide, silicon carbide, silicon and carbon in the Si-O-C system. So obviously, there are six different combinations in a divariant system with two condensed phases and a gas phase. It is known that carbon and silicon together can not be present at equilibrium conditions. This can be explained with reaction (2.3) which is impossible. If silicon is dissolved in iron, silicon can react with carbon.

Si + C = SiC (2.3)

According to the equilibrium, there can be five reactions and (2.4) is a solid-solid reaction that produces gases in form of SiO(g) and CO(g).

SiO_2 (s) + C (s) = SiO (g) + CO (g) (2.4)

If the activities of the condensed phases are set to one and the total pressure is 1 atmosphere, the divariant system can be determined. The following transformation sequence has been used to the calculation of the Si-O-C system. The temperatures of the phase transformation are respectively 848K, 1140K, 1738K[1].

α-Quartz → β-Quartz → HL-Tridymite → β-Cristobalite (2.10)

According to Scace and Slack (1959) SiC decomposes peritectically at 2830^{o}C, giving a liquid with 19 at% C, as seen in the phase diagram in Figure 2.2. The only one stable condensed compound in the system is SiC, which occurs in several hexagonal polytypes called α-SiC and one cubic modification called β-SiC. In accordance with the JANAF Thermochemical Tables (Chase 1985), the β-SiC is more stable than the α-SiC at all temperatures, but the difference is so small that it is not significant to

evaluate the equilibrium of this system[1].

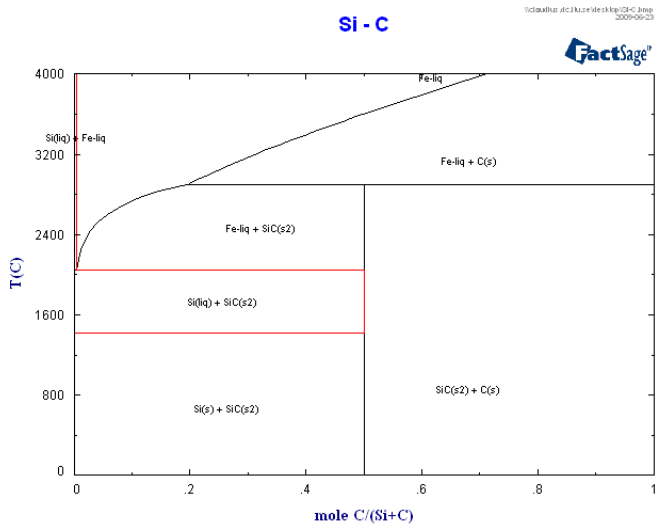

Figure 2.2 Phase diagram of Si-C system[8]

Reaction (2.4) begins below the triple point at approximately 1785K (1512^{o}C). Thermodynamically SiC can be formed above this temperatures according to reaction (2.5).

$$SiO\ (g) + 2C\ (s) = SiC\ (s) + CO\ (g) \qquad (2.5)$$

The equilibrium of the Si-C-O system is shown in Figure 2.3. The silicon carbide product reacts with quartz according to reaction (2.6) where two condensed phases are producing gaseous products. Produced silicon monoxide is more than carbon monoxide. Reaction (2.7) occurs at the second triple point where the temperature is 2084K (1811^{o}C). Reaction (2.8) takes place where silicon in its liquid phase reacts with quartz forming gaseous silicon monoxide. Figure 2.3 shows large number of information about the reduction path of the silicon dioxide[9].

$$2SiO_2\ (s) + SiC\ (s) = 3SiO\ (g) + CO\ (g) \qquad (2.6)$$

$$SiO\ (g) + SiC\ (s) = 2Si\ (l) + CO\ (g) \qquad (2.7)$$

$$SiO_2\ (s) + Si\ (l) = 2SiO\ (g) \qquad (2.8)$$

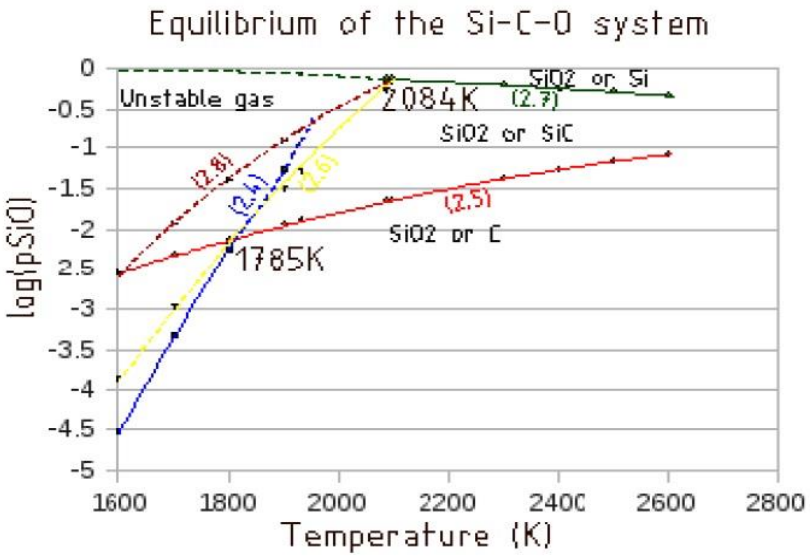

Figure 2.3 Equilibrium diagram of the Si-O-C system where the total pressure is set to 1 atmosphere[1].

2.3.2 The Fe-C-O system

Hematite (Fe_2O_3) is added to the system in a ferrosilicon furnace. Hematite react with carbon can be written as reaction (2.9).

$$Fe_2O_3\,(s) + 3C\,(s) = 2Fe\,(l) + 3CO\,(g) \quad (2.9)$$

The reaction (2.9) can be divided into three steps because hematite does not go directly to metallic iron. The first step is that Fe_2O_3 turns into Fe_3O_4 as reaction (2.11).

$$3Fe_2O_3\,(s) + CO\,(g) = 2Fe_3O_4\,(s) + CO_2 \quad (2.11)$$

The formed Fe_3O_4 would react further according to reaction (2.12) with carbon monoxide.

$$Fe_3O_4\,(s) + CO\,(g) = 3FeO\,(s) + CO_2\,(g) \quad (2.12)$$

The formed FeO could also go through a direct reduction with carbon (2.13) or an indirect reduction with carbon monoxide (2.14).

$$FeO\,(s) + C\,(s) = Fe\,(l) + CO\,(s) \quad (2.13)$$

$$FeO\,(s) + CO\,(g) = Fe\,(l) + CO_2\,(g) \quad (2.14)$$

Direct reduction with carbon is not thermodynamically advantageous but indirect reduction with carbon monoxide is more seemly to happen. Carbon dioxide can react with carbon as reaction (2.15) since carbon oxide is not stable at high temperature.

$$CO_2\ (g) + C\ (s) = 2CO\ (g) \quad (2.15)$$

2.3.3 Solution of silicon into molten iron

Molten iron dissolves carbon and carbon-saturated iron may be formed as low as at 1153^{o}C[1]. Then SiO-containing gas can react and take silicon into the solution (2.16)[10].

$$SiO\ (g) + C_{Fe} = Si_{Fe} + CO\ (g) \quad (2.16)$$

The silicon solubility in iron solution at temperature below 1512^{o}C is evaluated by the equilibrium of the reaction (2.17).

$$SiO_2 + 2C\ (s) = Si_{Fe} + 2CO\ (g) \quad (2.17)$$

When the temperature is between 1512^{o}C and 1811^{o}C, the equilibrium is defined by reaction (2.18)[1].

$$SiO_2 + 2SiC\ (s) = 3Si_{Fe} + 2CO\ (g) \quad (2.18)$$

2.3.4 Reactions in the furnace

Combining the theory of the Si-O-C system and Fe-C-O system, large numbers of different reactions are taken place in the furnace. Additional reactions like (2.19) and (2.20) take place at the surface. These reactions will occur because there would be always air present on the top of the charge. Especially when the gates are open, these reactions can be easily taken place.

$$SiO\ (g) + 1/2\ O_2\ (g) = SiO_2\ (s) \quad (2.19)$$

$$CO\ (g) + 1/2\ O_2\ (g) = CO_2\ (g) \quad (2.20)$$

The boudard reaction (2.15) is a well-known reaction and occurs at temperature above

1000°C.

CO_2 (g) + C (s) = 2CO (g) (2.15)

The CO and SiO gases would go through the material bed and not only react with iron oxide but also react with carbon material to form SiC (2.21). And the two gases can react with themselves as the reaction (2.22).

3SiO (g) + CO (g) = $2SiO_2$ (s) + SiC (s) (2.21)

SiO (g) + CO (g) = SiO_2 (s) + C (s) (2.22)

Silicon is produced as predicted from the idealized overall reaction (2.23) of the process.

SiO_2 (s) + 2C (s) = Si (l) + 2CO (g) (2.23)

And there are also some undesired reactions (2.24, 2.25) in the furnace.

SiO_2 (s) + C (s) = SiO (g) + CO (g) (2.24)

SiO_2 (s) +3C (s) = SiC (s) + 2CO (g) (2.25)

The three reactions all can be seen as SiO_2 (s) + xC (g). From these reactions, adding less carbon than optimal carbon coverage will result in excessive formation of gas and hence reduced silicon recovery because of the loss of SiO gas. This is known from (2.24). On the contrary, from reaction (2.25), addition of too much carbon will result in accumulation of SiC in the furnace which is also causing a reduction in the silicon recovery. Association between carbon coverage and silicon recovery is shown in Figure 2.4. It is quite essential to control carbon coverage in the silicon furnace.

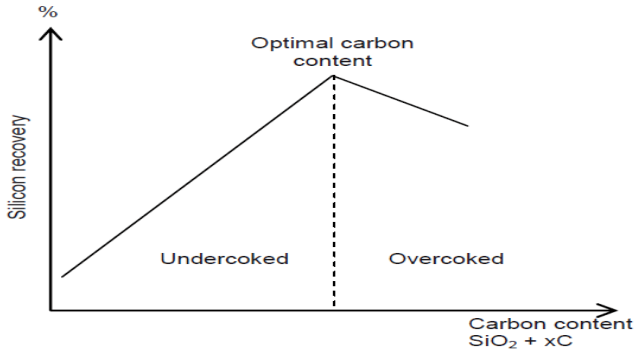

Figure 2.4 Silicon recovery as a function of the carbon content in the charge. Modified after Valderhaug (1992)[4].

The temperature is between 1790-2050^{o}C at the depth of 1.5m to 1.9m[1]. In this temperature zone, molten silicon dioxide would probably be seen. The previously formed SiC can react according to reaction (2.7) at temperature above 1811^{o}C[1]. The silicon producing reaction (2.26) is evaluated by the combination of three reactions (2.6, 2.7, 2.8).

$$3SiO_2\ (l) + 2SiC\ (s) = Si\ (l) + 4SiO\ (g) + 2CO\ (g) \qquad (2.26)$$

Metallic iron has been in its molten phase with dissolved silicon according to reactions (2.16, 2.17, 2.18). Then it would sink to the bottom of the furnace as a metallic bath containing Fe_xSi_y which depends on the composition of Fe and Si[3].

The temperature is between 2050-2190^{o}C at the depth of 1.9m to 2.7m[1]. Below is the inner structure of the submerged are furnace shown in Figure 2.5. In this figure, the temperatures in different zone are briefly shown.

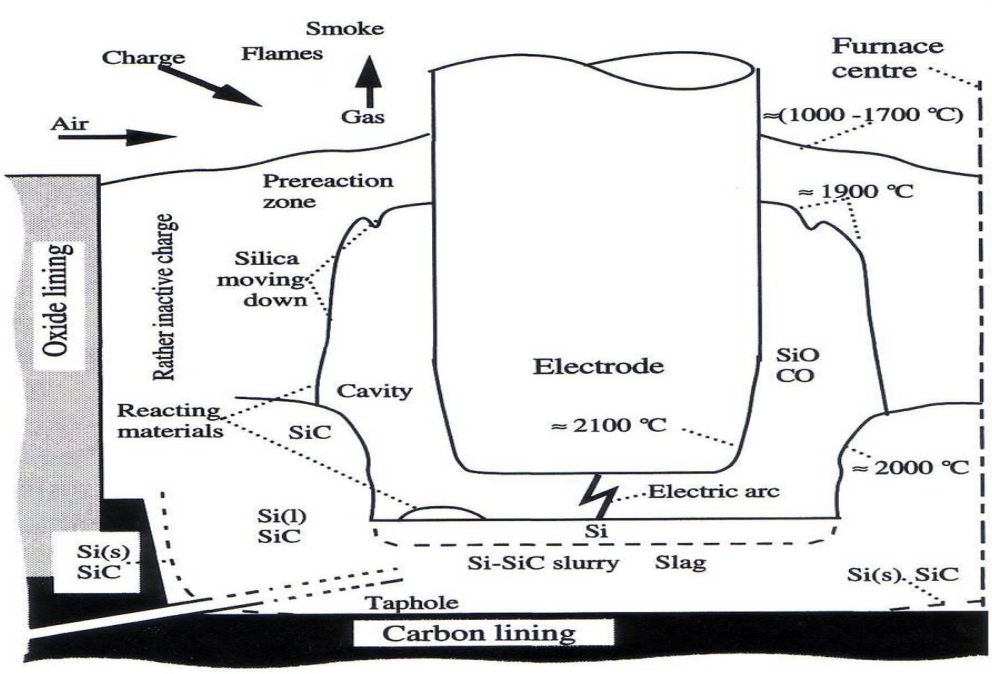

Figure 2.5 Inner structure of the submerged arc furnace[1]

3 Experimental work

3.1 Equipment

3.1.1 Light Optical Microscope

The light optical microscope is an instrument which is applied in observing the sample surface. It is a simple instrument which can investigate different phases of samples. During the observation, different phases can be determined because dense material like metals can reflect more light than oxides and carbides. The micro pictures of each prepared samples were taken by LOM to provide the direction for further research.

Below is a view of the instrument.

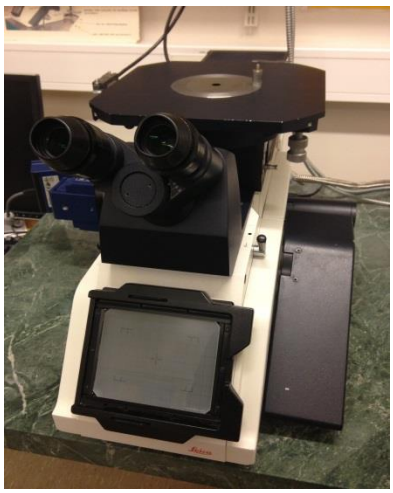

Figure 3.1 LOM instrument Leica MEF4M

3.1.2 Scanning Electron Microscope[11]

In this project, SEM equipment is Hitachi SU-6600 (Figure 2.1). Hitachi's SU6600 is a new SEM for widely applied in observing and analysing advanced materials. SEM images can be in very high magnification rate to show different phases and structures of the samples clearly[12]. Accelerating voltage was set to 15kV during this work.

The better electric conductivity of the sample gets the better quality in SEM image.

Figure 3.2 SEM equipment Hitachi SU-6600

3.1.3 Energy Dispersive X-ray Spectrometer

EDS is an analytical technique used for the elemental analysis or chemical characterization of a sample. It relies on the investigation of an interaction of some source of X-ray excitation and a sample. Its characterization capabilities are due to the fundamental principle that each element has a unique atomic structure allowing unique set of peaks on its X-ray spectrum. In this project, EDS analysis was also on the Hitachi SU-6600 equipment[12].

3.1.4 Electron Probe Micro Analysis

EPMA is based on electron bombardment to generate X-rays in the sample that is going to be analysed. The elements present and their concentrations may be estimated and identified from the intensity and wavelength of the lines in the X-ray spectrum. The electron beam is finely focused so that it can do analyses on very small selected area[13].

In this project the EPMA instrument is JXA-8500F. The JXA-8500F is a high

performance thermal field emission electron probe micro analyzer combining high SEM resolution with high quality X-ray analysis of submicron areas. The JEOL JXA-8500F instrument is equipped with 5 wavelength dispersive X-ray spectrometers (WDS) and an energy dispersive X-ray spectrometer (EDS). This combination can simultaneously analyses 5 elements WDS + 16 elements EDS plus collect image signals from backscatter and secondary electron detectors. The magnification rate is from 40x to 300,000x. Below is a view of the instrument[14].

Figure 3.3 EPMA instrument JXA-8500F

3.1.5 X-Ray Diffraction

XRD is an instrument which can be used to reveal information about sample's crystal structure and chemical composition. The most intense reflection by the X-rays can determine their d-spacing. The corresponding d-values can be searched in reference in computer software. X-radiation is diffracted into well-defined directions by the atoms of crystalline materials. The peak positions and intensities are given by the crystal structure (symmetry, dimensions, and atomic positions of the crystal unit cell). They are characteristic for every crystalline compound and allow phase identification. In this project, the X-ray diffractometer is Siemens A unit. The samples were scanned over an angular area of sin2θ 5-70^{o} with 0.02^{o}θ per step and 0.04 seconds per step.

Figure 3.4 XRD equipment Siemens A Unit

3.2 Samples

3.2.1 Sample selection

In 2009, an industrial FeSi furnace was excavated and more than 130 samples at different locations in the furnace collected. Samples were divided into four parts which are furnace top, cross-section X, cross-section Y and cross-section Z (Figure 3.5). For the present study, ten samples were selected according to the samples' location in the furnace and estimated composition. Because the ten selected samples were located in different locations in the ferrosilicon furnace and had different compositions, they can reflect some behaviour of the elements and show the total furnace reactions from their deeper investigation.

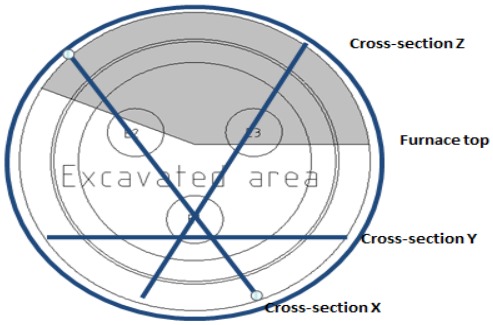

Figure 3.5 Overview from the furnace top

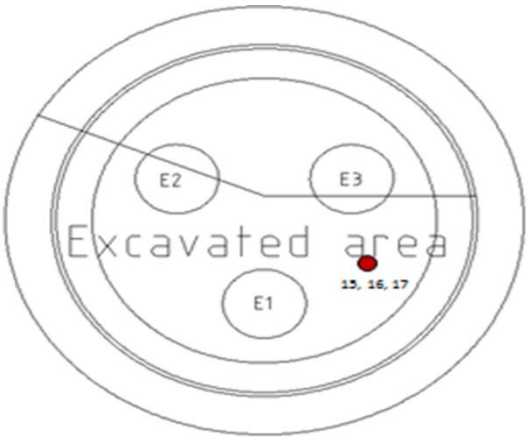

Figure 3.6 Furnace top

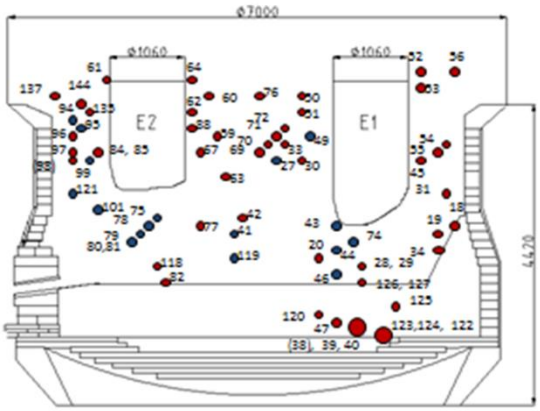

Figure 3.7 Cross-section X

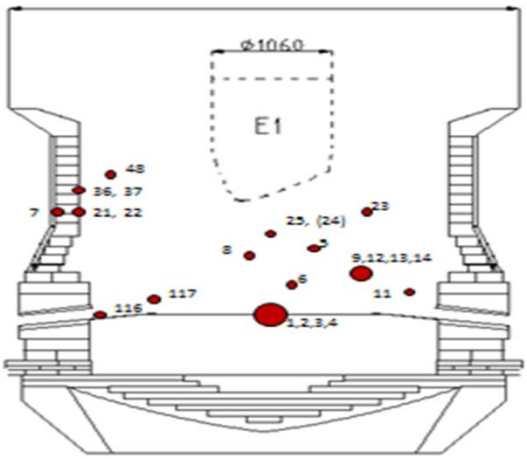

Figure 3.8 Cross-section Y

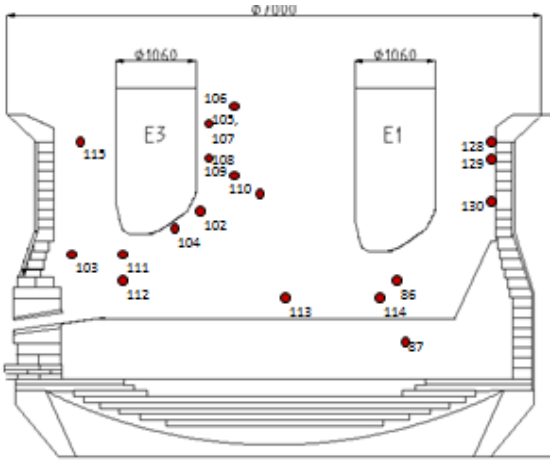

Figure 3.9 Cross-section Z

3.2.2 Preparation

The samples need to be a flat smooth surface because a slightly slope of 1^{o} may change the absorption correction and backscattering to cause a deviation.

Selected samples were mounted in epoxy. After that, samples were ground and polished until surface particle diameter is 1μm. These were preparation for future XRD, SEM, EDS and EPMA work. The grinding work was done on a grinding machine with SiC paper or Diamond Pad. The polishing was done with a similar machine as grinding machine but on a rotating nylon cloth laps with corresponding diamond polishing paste. Below is a picture of some prepared samples (Figure 3.10).

Figure 3.10 Prepared samples

A conducting path should be available on the specimen to provide electric conduction from the probe to the earth. Because the samples do not have very good electrical conductivity, they were carbon coated in order to do the EPMA work. However, the non-coated samples were used to do the XRD, SEM and EDS work because additional carbon can cause a big deviation and make the analysing work much more difficult. It was also the reason why some microscope pictures did not have very good quality.

4 Results

The results consist of analysis of selected samples. Samples for XRD, SEM and EDS analysis were not carbon-coated in order to get a good data for carbon element. And it led to some image quality was not so good. Samples for EPMA analysis were carbon-coated.

Below are sample No.15’s location and analysis data. It was excavated from the furnace top.

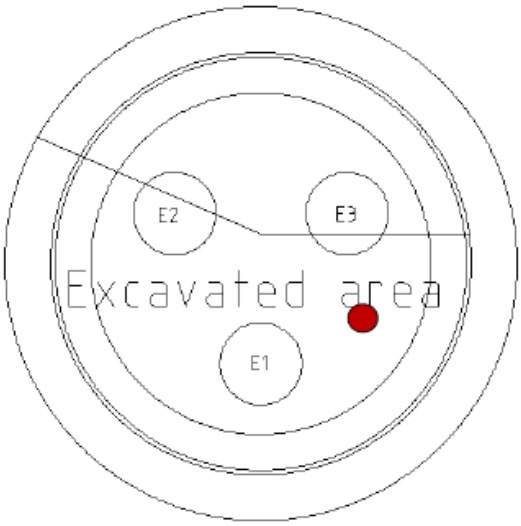

Figure 4.1 Sample No.15's location

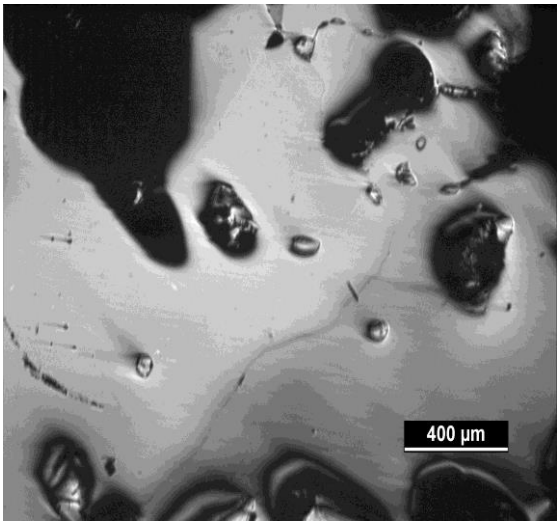

Figure 4.2 Sample No.15's micro picture

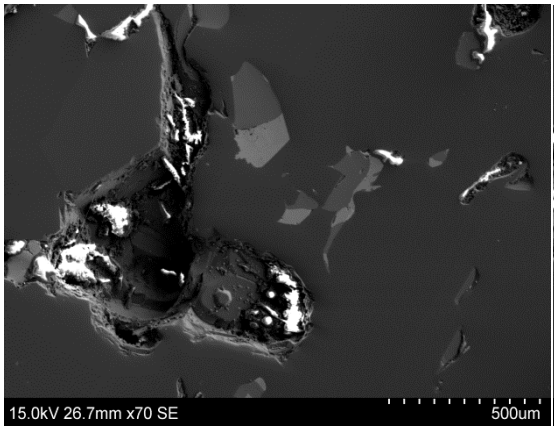

Figure 4.3 SEM image at 70x magnification

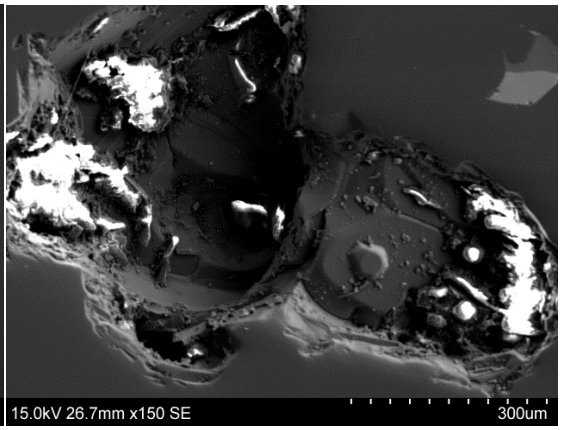

Figure 4.4 SEM image at 150x magnification

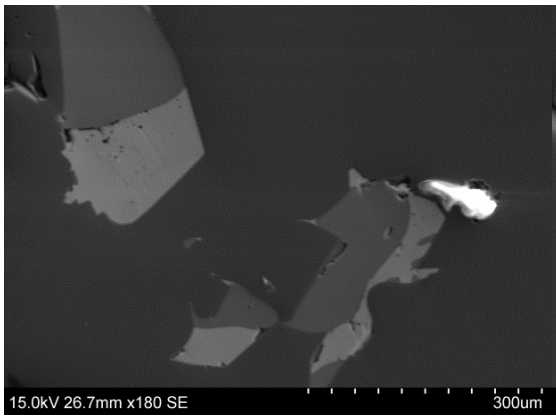

Figure 4.5 SEM image at 180x magnification

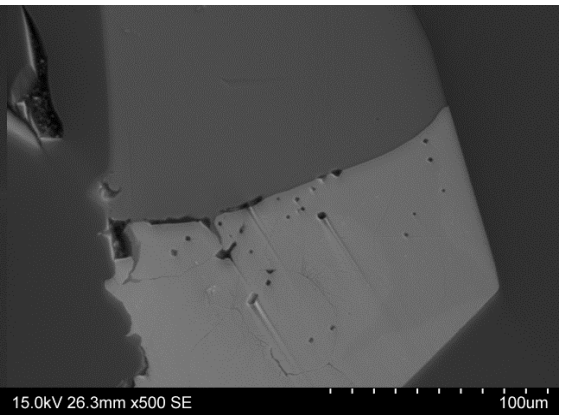

Figure 4.6 SEM image at 500magnification

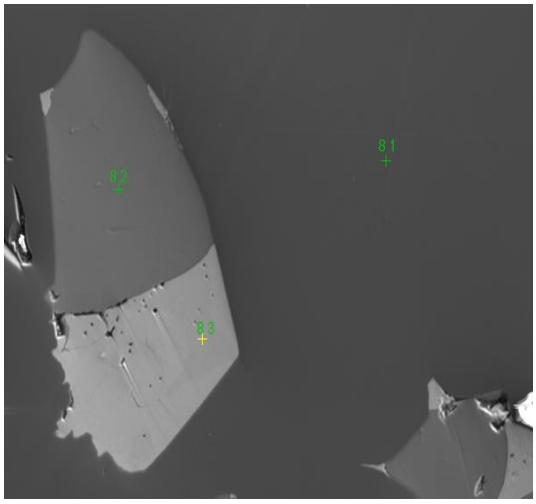

Figure 4.7 EDS image at 250x magnification

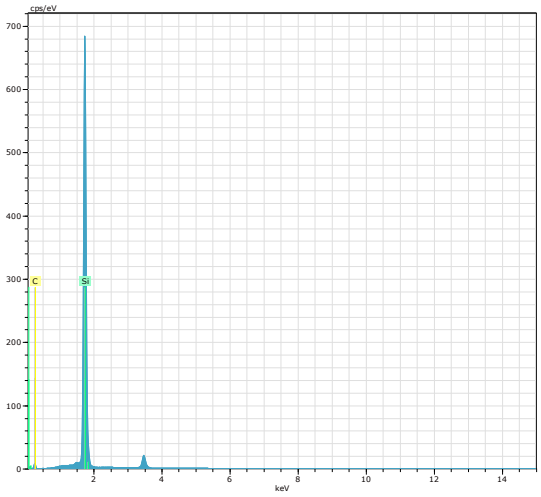

Figure 4.8 EDS graph for point 8 1

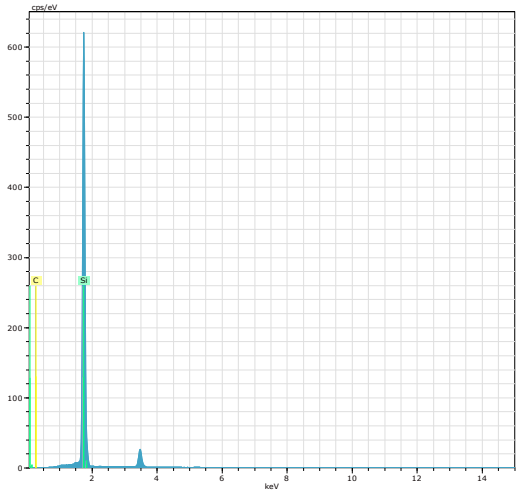

Figure 4.9 EDS graph for point 8 2

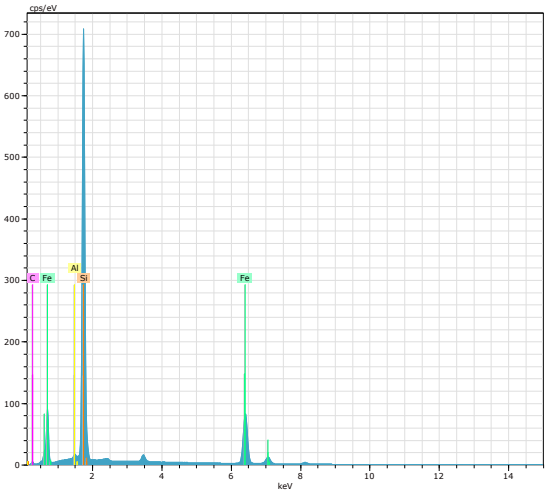

Figure 4.10 EDS graph for point 8 3

Table 4.1 EDS analysis data for point 8 1

El	AN	Series	unn. C [wt.%]	norm. C [wt.%]	Atom. C [at.%]	Error (1 Sigma) [wt.%]
C	6	K-series	12,29	16,97	32,33	1,45
Si	14	K-series	60,15	83,03	67,67	2,52
		Total:	72,44	100,00	100,00	

Table 4.2 EDS analysis data for point 8 2

El	AN	Series	unn. C [wt.%]	norm. C [wt.%]	Atom. C [at.%]	Error (1 Sigma) [wt.%]
C	6	K-series	1,92	2,52	5,70	0,37
Si	14	K-series	74,31	97,48	94,30	3,11
		Total:	76,23	100,00	100,00	

Table 4.3 EDS analysis data for point 8 3

El AN	Series	unn. C [wt.%]	norm. C [wt.%]	Atom. C [at.%]	Error (1 Sigma) [wt.%]
C 6	K-series	2,35	2,68	7,90	0,34
Al 13	K-series	0,40	0,45	0,59	0,04
Si 14	K-series	42,09	47,97	60,49	1,77
Fe 26	K-series	42,91	48,90	31,02	1,28
	Total:	87,75	100,00	100,00	

From these analysis data, sample No.15 is mainly composed by silicon carbide (Point 8 1), silicon (Point 8 2), ferrosilicon (Point 8 3). Because the atomic number of carbon is six, carbon percentages which were calculated from EDS analysis have a quite large error.

Below are sample No.25's location and analysis data.

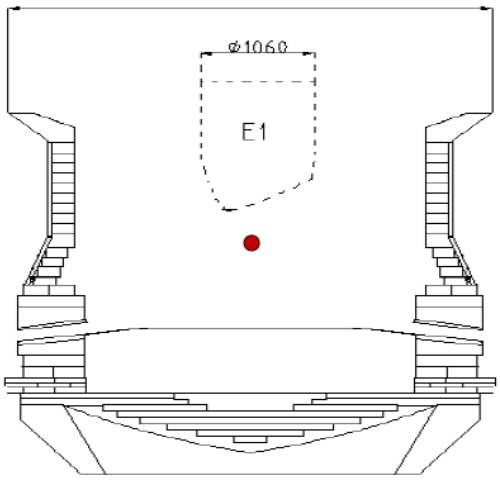

Figure 4.11 Sample No.25's location

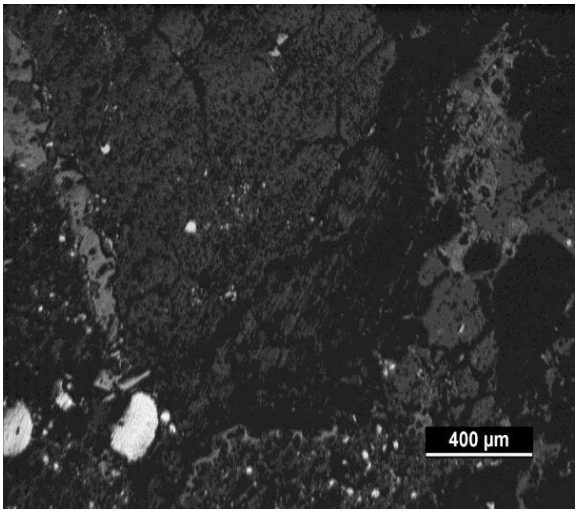

Figure 4.12 Sample No.25's micro picture

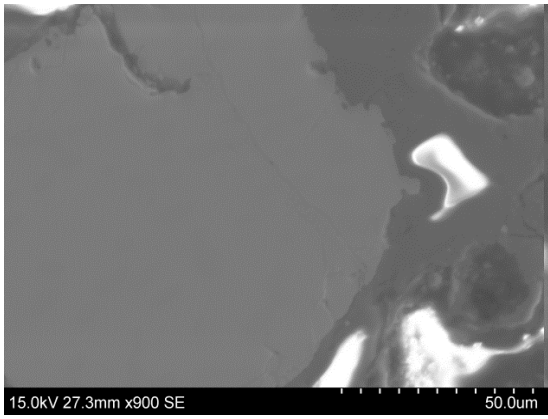

Figure 4.13 SEM image at 900x magnification

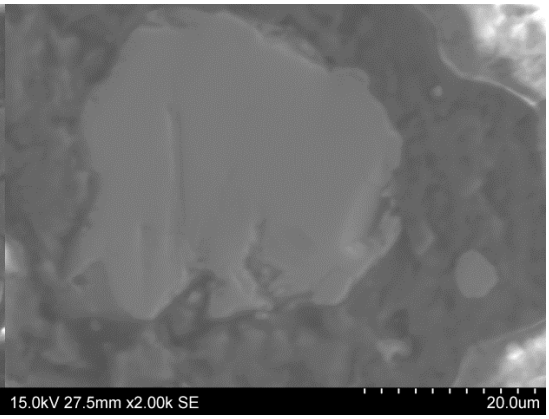

Figure 4.14 SEM image at 2000x magnification

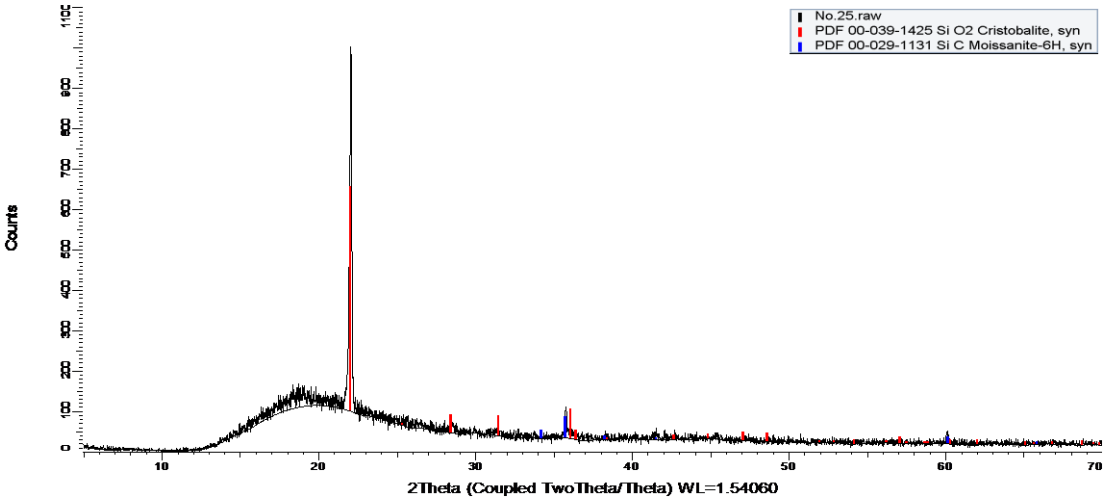

Figure 4.15 Sample No.25's XRD graph

From these images and XRD graph, the sample No.25 is mainly composed by SiO_2 and silicon carbide with several small dots of ferrosilicon phases. In the XRD graph, the background at the beginning of the scanning was not stable. The main reason was that the samples were mounted in epoxy.

Below are sample No.48's location and analysis data. The sample is a condensate and locates 40cm from the outer wall.

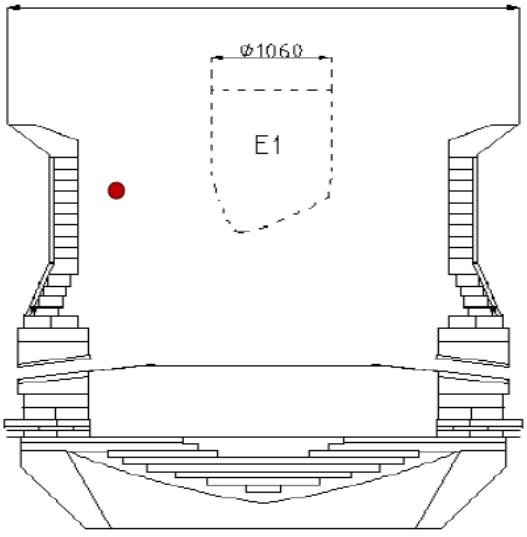

Figure 4.16 Sample No.48's location

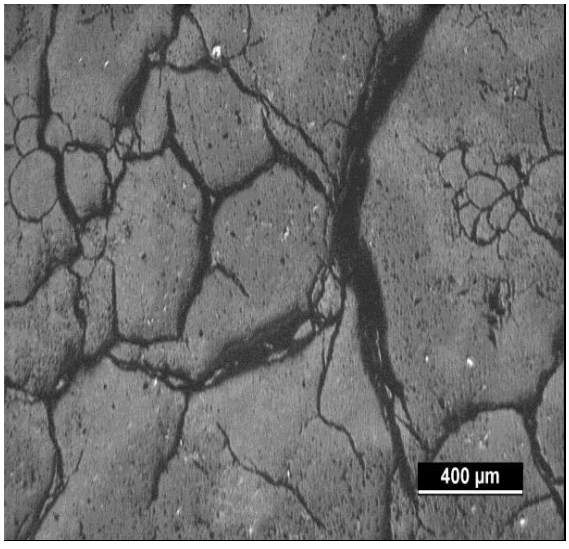

Figure 4.17 Sample No.48's micro picture

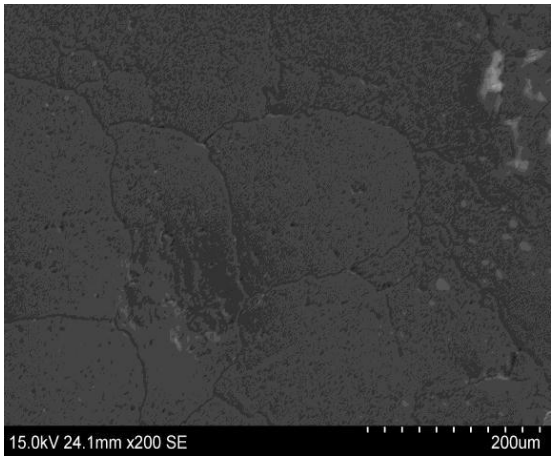

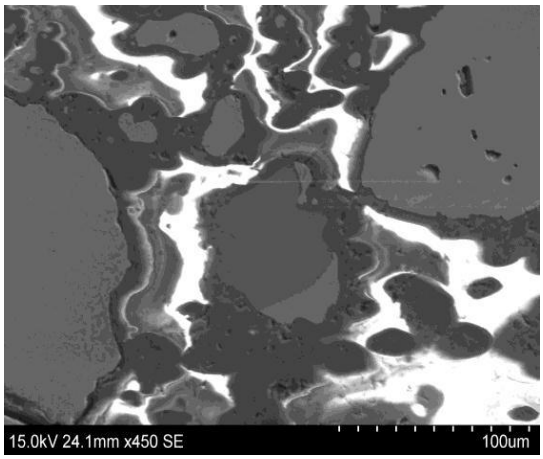

Figure 4.18 SEM image at 200x magnification Figure 4.19 SEM image at 450x magnification

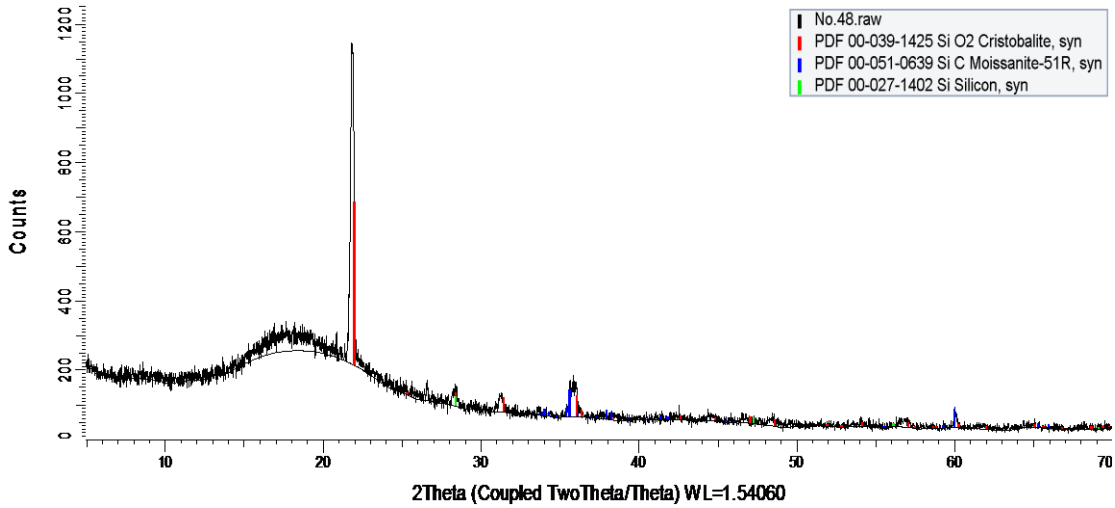

Figure 4.20 Sample No.48's XRD graph

From these images and XRD graph, the sample No.48 is mainly composed by SiO_2 and silicon carbide with some silicon and ferrosilicon metal phases. In the XRD graph, the background at the beginning of the scanning was not stable. The main reason was that the samples were mounted in epoxy.

Below are sample No.49's location and analysis data. The sample was excavated from Cross-section X and it was close to electrode 1.

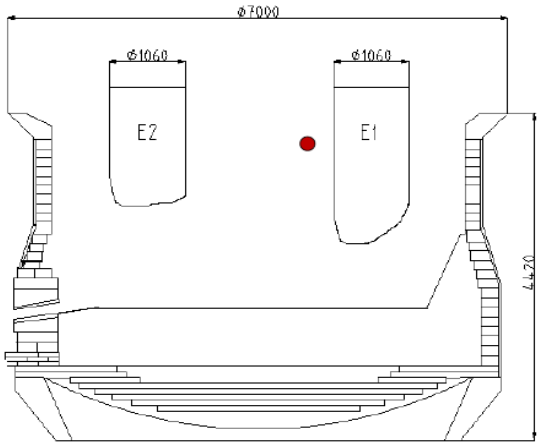

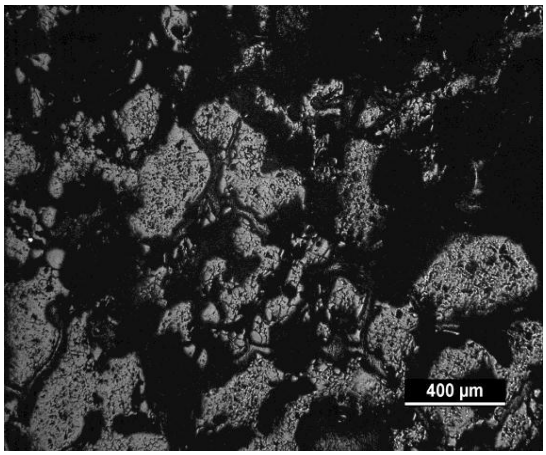

Figure 4.21 Sample No.49's location

Figure 4.22 Sample No.49's micro picture

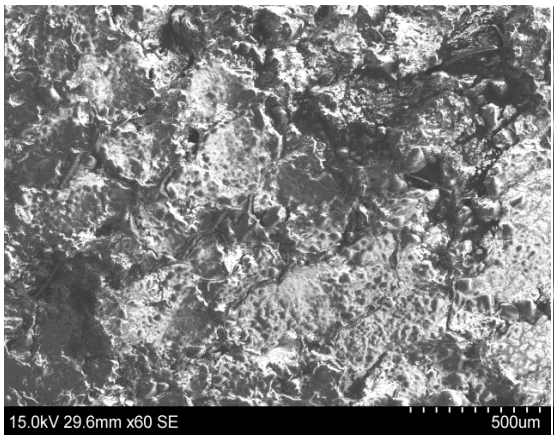

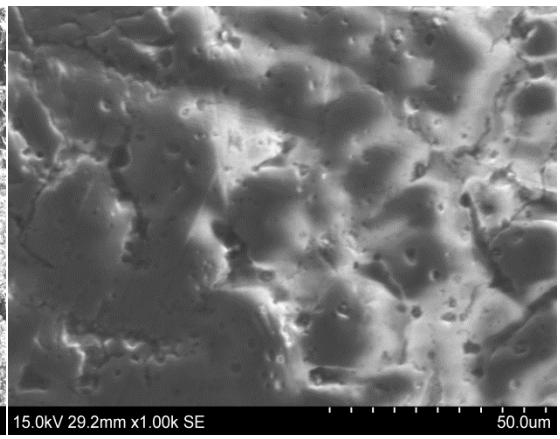

Figure 4.23 SEM image at 60x magnification Figure 4.24 SEM image at 1000x magnification

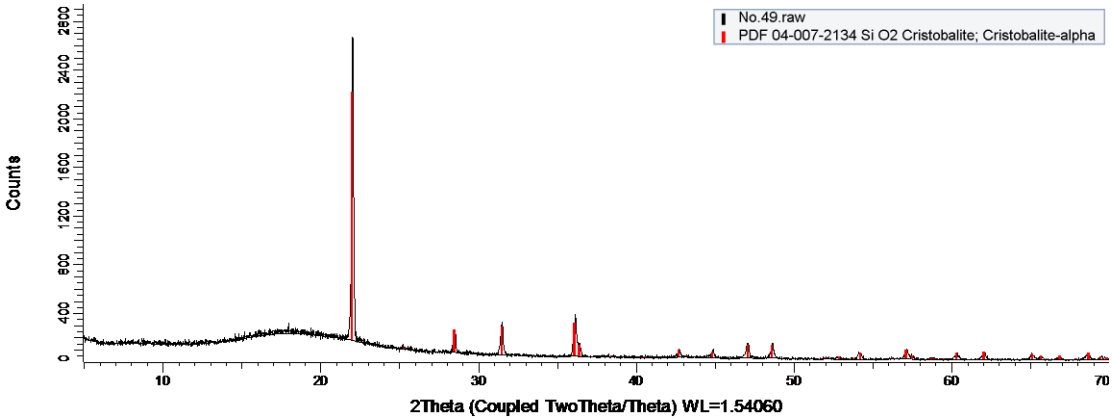

Figure 4.25 Sample No.49's XRD graph

From these images and XRD graph, the sample No.49 is quartz which is α-cristobalite. In the XRD graph, the background at the beginning of the scanning was not stable. The main reason was that the samples were mounted in epoxy.

Below are sample No.74's location and analysis data. The sample was excavated from 95 cm below the electrode 1's tip.

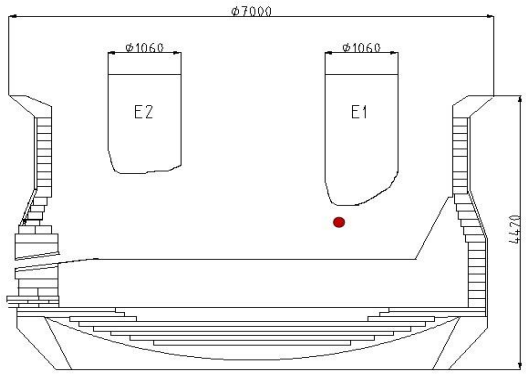

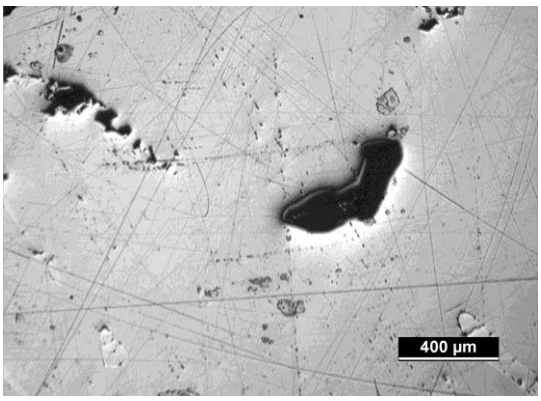

Figure 4.26 Sample No.74's location

Figure 4.27 Sample No.74's micro picture

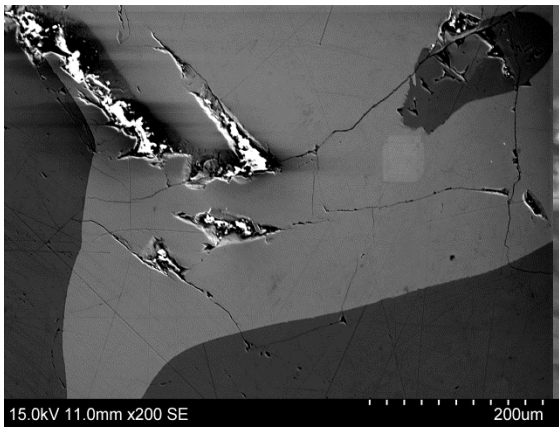

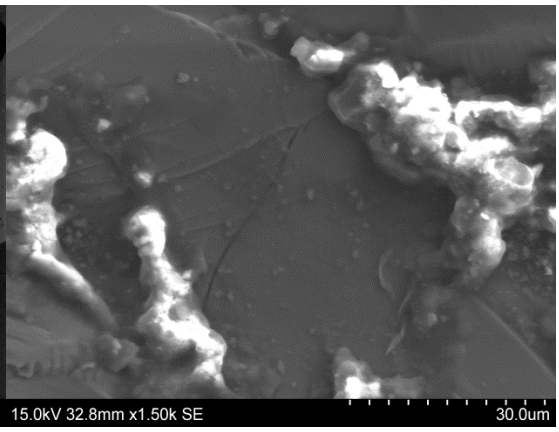

Figure 4.28 SEM image at 200x magnification

Figure 4.29 SEM image at 1500x magnification

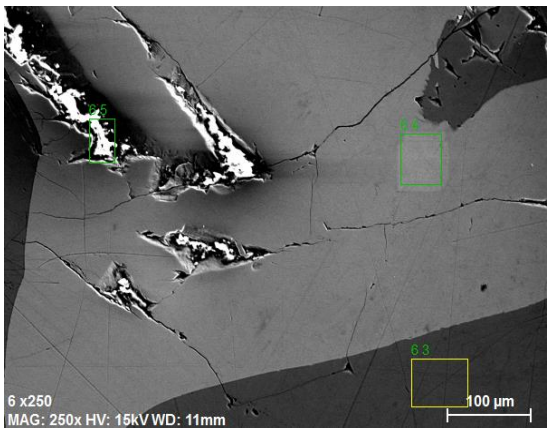

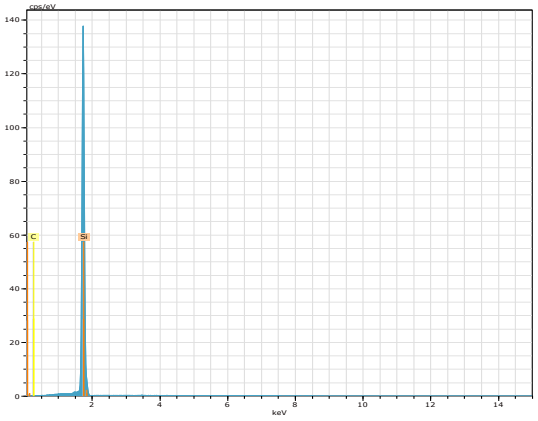

Figure 4.30 EDS image at 250x magnification

Figure 4.31 EDS graph for area 6 3

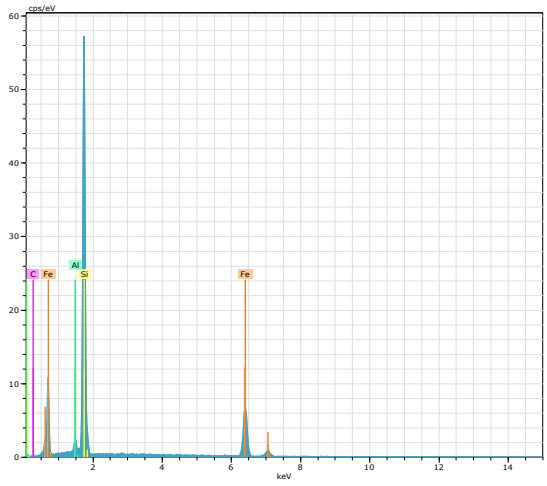

Figure 4.32 EDS graph for area 6 4

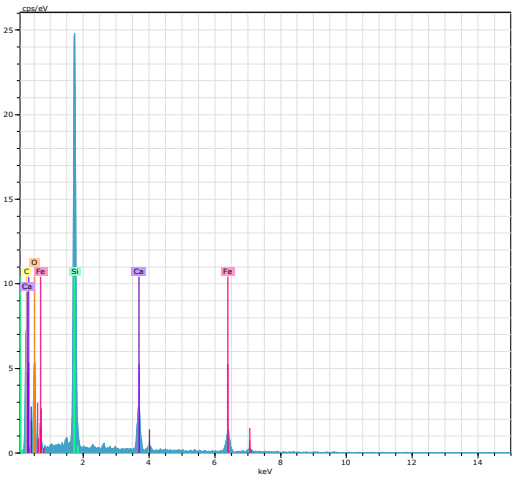

Figure 4.33 EDS graph for area 6 5

Table 4.4 EDS analysis data for area 6 3

El	AN	Series	unn. C [wt.%]	norm. C [wt.%]	Atom. C [at.%]	Error (1 Sigma) [wt.%]
Si	14	K-series	102,30	96,12	91,38	4,28
C	6	K-series	4,13	3,88	8,62	1,35
		Total:	106,43	100,00	100,00	

Table 4.5 EDS analysis data for area 6 4

El	AN	Series	unn. C [wt.%]	norm. C [wt.%]	Atom. C [at.%]	Error (1 Sigma) [wt.%]
Si	14	K-series	52,31	51,45	63,31	2,22
Fe	26	K-series	45,23	44,49	27,53	1,43
C	6	K-series	2,52	2,48	7,14	0,99
Al	13	K-series	1,60	1,58	2,02	0,12
		Total:	101,66	100,00	100,00	

Table 4.6 EDS analysis data for area 6 5

El	AN	Series	unn. C [wt.%]	norm. C [wt.%]	Atom. C [at.%]	Error (1 Sigma) [wt.%]
C	6	K-series	36,55	36,36	54,30	6,81
Si	14	K-series	25,48	25,35	16,19	1,13
O	8	K-series	20,56	20,45	22,93	3,94
Fe	26	K-series	11,14	11,08	3,56	0,51
Ca	20	K-series	6,79	6,75	3,02	0,29
		Total:	100,52	100,00	100,00	

This sample is a metal. It has pure silicon phase, ferrosilicon phase and some other metal phases which contain Al and Ca elements. Because the atomic number of

carbon is six, carbon percentages which were calculated from EDS analysis have a quite large error.

Below are sample No.75's location and analysis data. The sample was excavated from 15cm below electrode 2's tip.

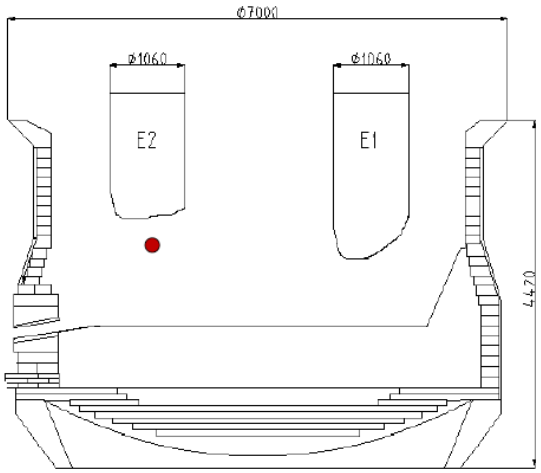

Figure 4.34 Sample No.75's location

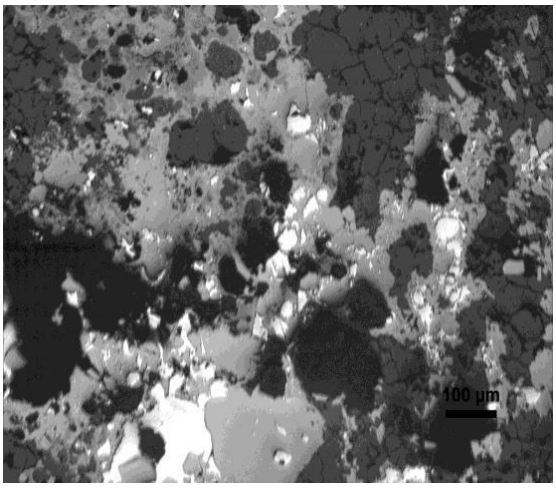

Figure 4.35 Sample No.75's micro picture

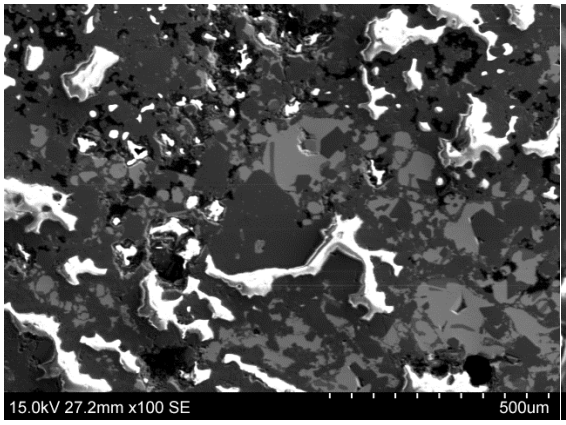

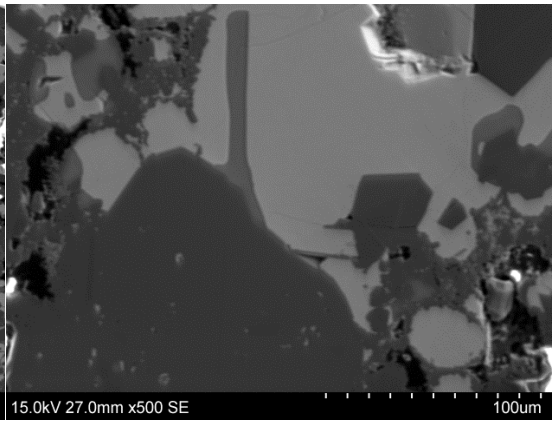

Figure 4.36 SEM image at 100x magnification Figure 4.37 SEM image at 500x magnification

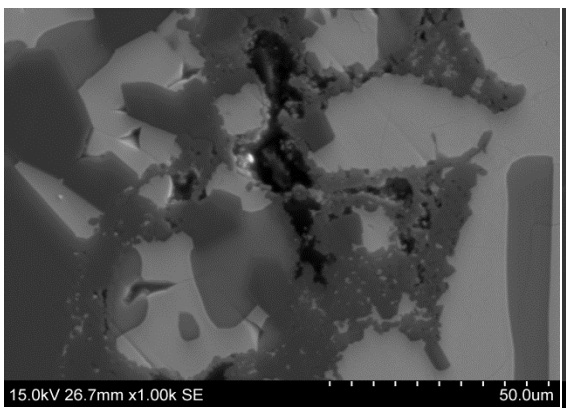

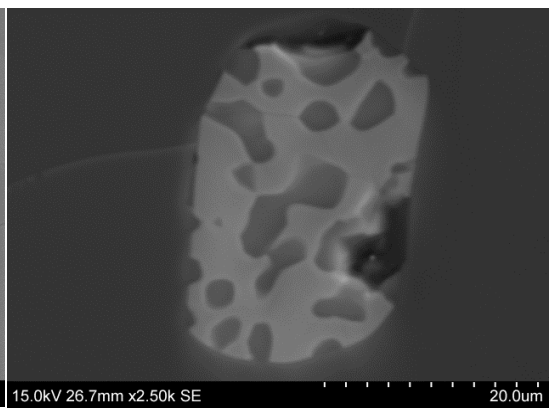

Figure 4.38 SEM image at 1000x magnification Figure 4.39 SEM image at 2500x magnification

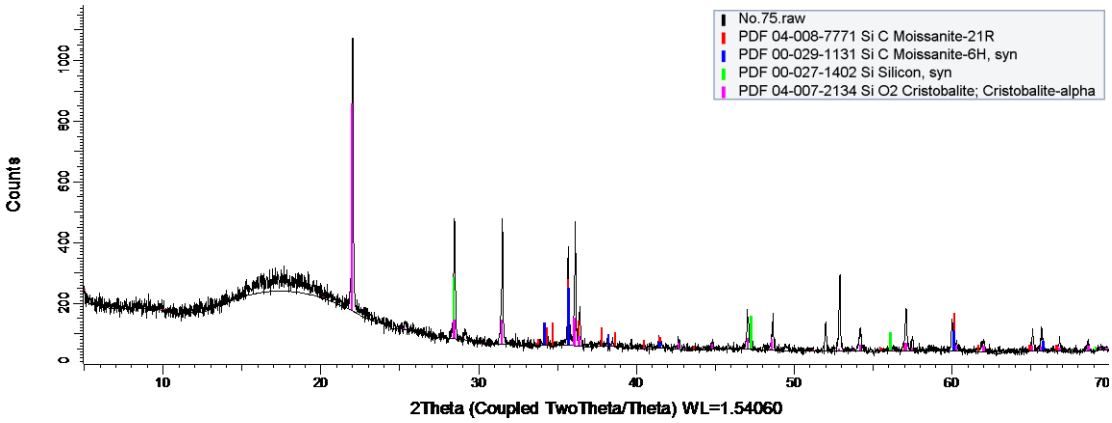

Figure 4.40 Sample No.75's XRD graph

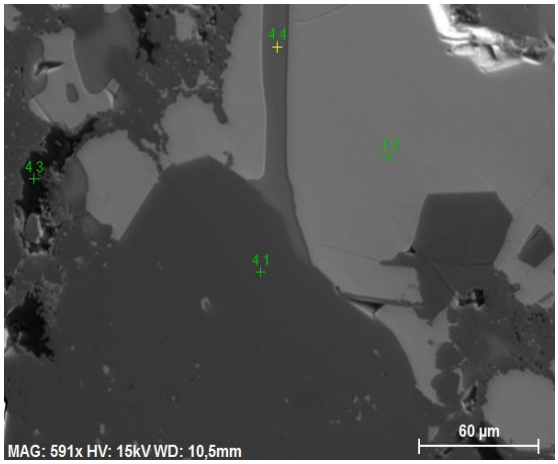

Figure 4.41 EDS image at 591x magnification

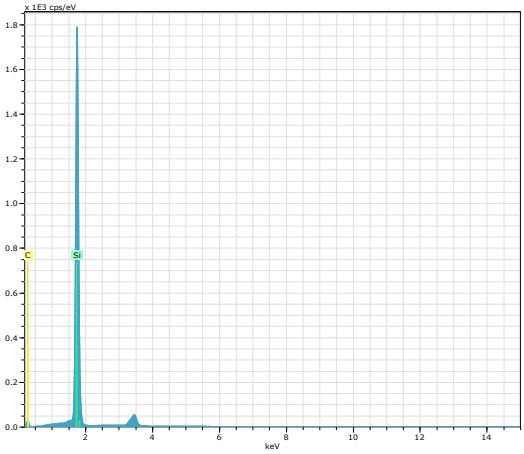

Figure 4.42 EDS graph for point 4 1

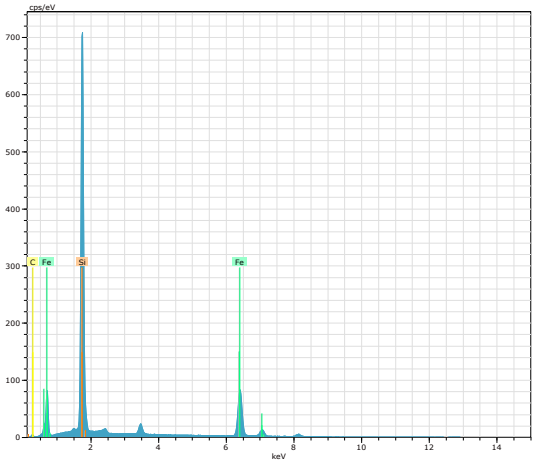

Figure 4.43 EDS graph for point 4 2

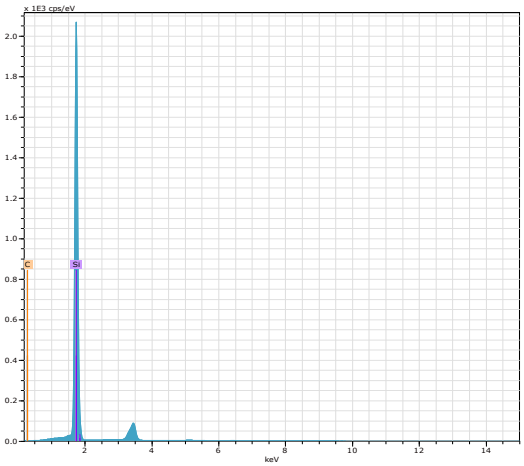

Figure 4.44 EDS graph for 4 4

Table 4.7 EDS analysis data for point 4 1

El	AN	Series	unn. C	norm. C	Atom. C	Error (1 Sigma)
			[wt.%]	[wt.%]	[at.%]	[wt.%]
C	6	K-series	17,15	21,90	39,60	1,95

Si	14	K-series	61,16	78,10	60,40	2,56
		Total:	78,31	100,00	100,00	

Table 4.8 EDS analysis data for point 4 2

El	AN	Series	unn. C	norm. C	Atom. C	Error (1 Sigma)
			[wt.%]	[wt.%]	[at.%]	[wt.%]
C	6	K-series	1,98	2,49	7,36	0,35
Si	14	K-series	38,82	48,68	61,58	1,64
Fe	26	K-series	38,95	48,84	31,07	1,16
		Total:	79,75	100,00	100,00	

Table 4.9 EDS analysis data for point 4 4

El	AN	Series	unn. C	norm. C	Atom. C	Error (1 Sigma)
			[wt.%]	[wt.%]	[at.%]	[wt.%]
C	6	K-series	3,84	4,86	10,68	0,53
Si	14	K-series	75,09	95,14	89,32	3,14
		Total:	78,93	100,00	100,00	

From these analysis data, sample No.75 is mainly composed by silicon carbide (Point 4 1), ferrosilicon (Point 4 2) and silicon (Point 4 4). Because the atomic number of carbon is six, carbon percentages which were calculated from EDS analysis have a quite large error. In the XRD graph, the background at the beginning of the scanning was not stable. The main reason was that the samples were mounted in epoxy.

Below are sample No.82's location and analysis data. The sample was excavated from 40cm below electrode 2's tip.

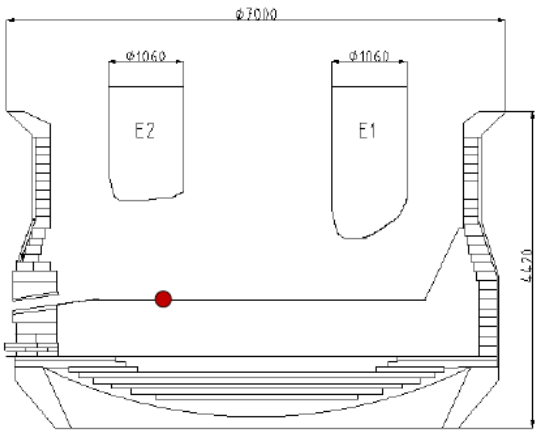

Figure 4.45 Sample No.82's location

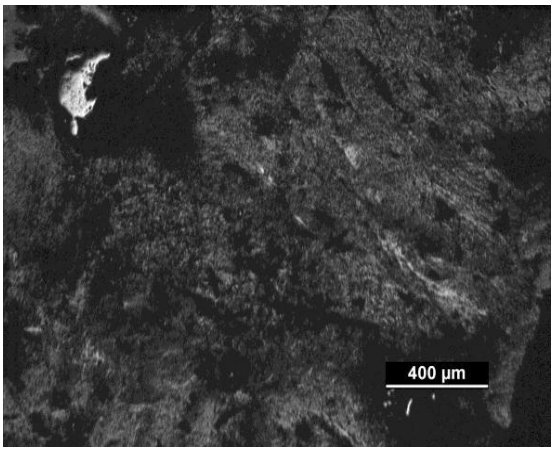

Figure 4.46 Sample No.82's micro picture

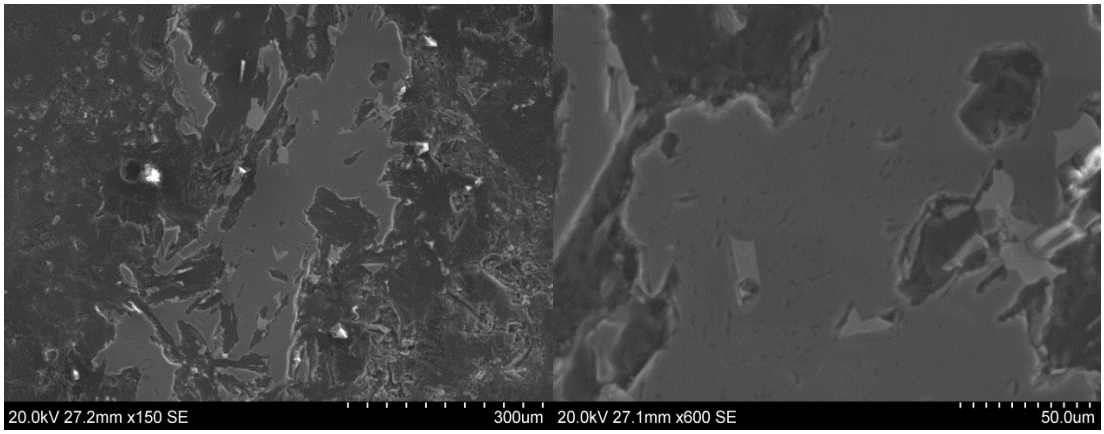

Figure 4.47 SEM image at 150x magnification Figure 4.48 SEM image at 600x magnification

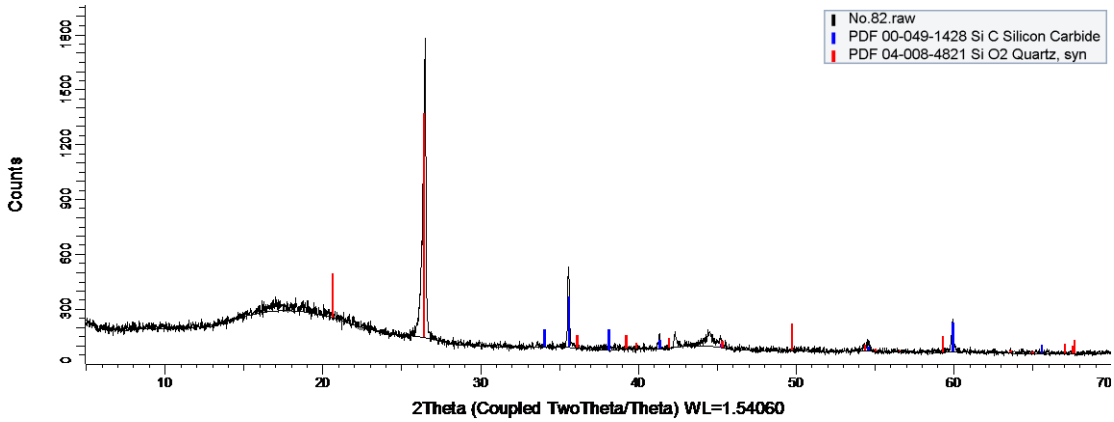

Figure 4.49 Sample No.82's XRD graph

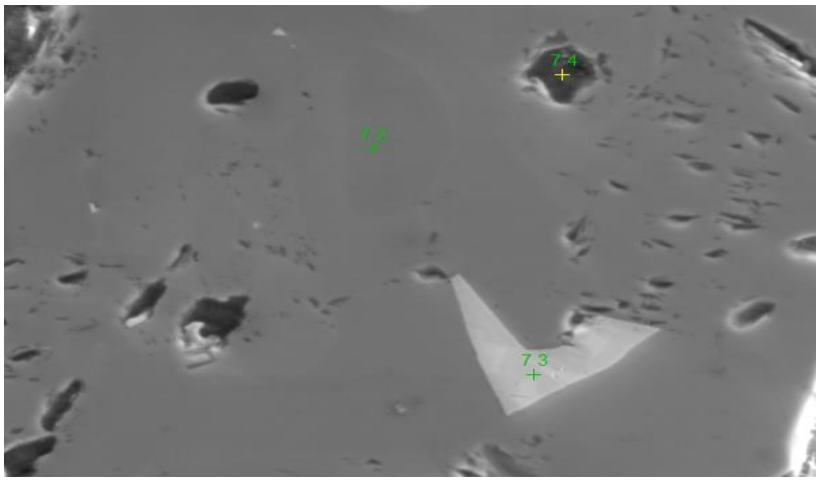

Figure 4.50 EDS image at 1200x magnification

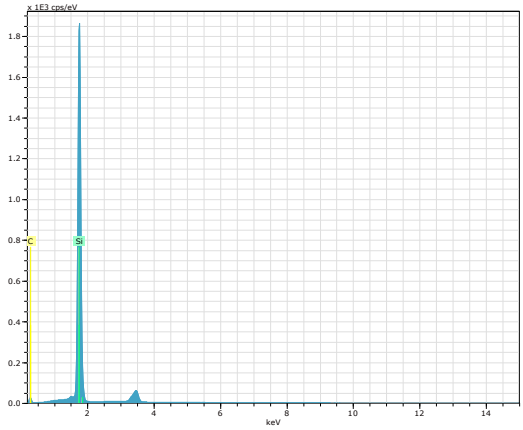

Figure 4.51 EDS graph for point 7 2

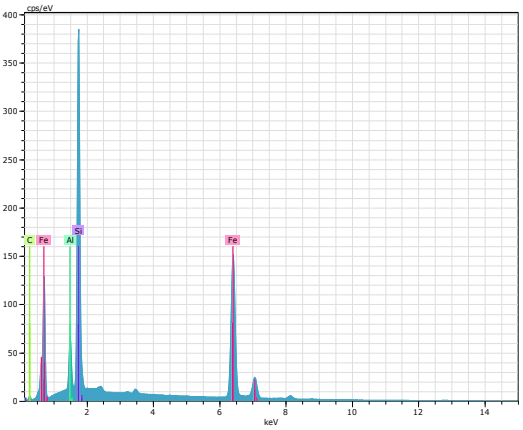

Figure 4.52 EDS graph for point 7 3

Table 4.10 EDS analysis data for point 7 2

El	AN	Series	unn. C	norm. C	Atom. C	Error (1 Sigma)
			[wt.%]	[wt.%]	[at.%]	[wt.%]
C	6	K-series	15,18	20,73	37,95	1,77
Si	14	K-series	58,03	79,27	62,05	2,43
		Total:	73,21	100,00	100,00	

Table 4.11 EDS analysis data for point 7 3

El	AN	Series	unn. C	norm. C	Atom. C	Error (1 Sigma)
			[wt.%]	[wt.%]	[at.%]	[wt.%]
C	6	K-series	0,85	1,05	3,72	0,16
Al	13	K-series	2,88	3,57	5,61	0,16
Si	14	K-series	19,54	24,20	36,57	0,84
Fe	26	K-series	57,46	71,18	54,10	1,70
		Total:	80,73	100,00	100,00	

From these analysis data, sample No.82 is mainly composed by silicon carbide, silicon and silica with some small dots of ferrosilicon. Because the atomic number of carbon is six, carbon percentages which were calculated from EDS analysis have a quite large error. In the XRD graph, the background at the beginning of the scanning was not stable. The main reason was that the samples were mounted in epoxy.

Below are sample No.106's location and analysis data.

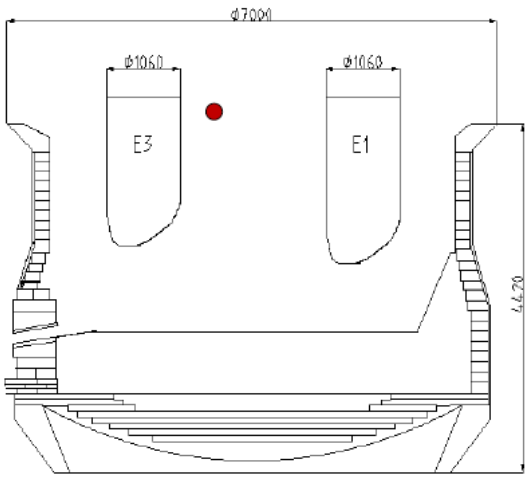

Figure 4.53 Sample No.106's location

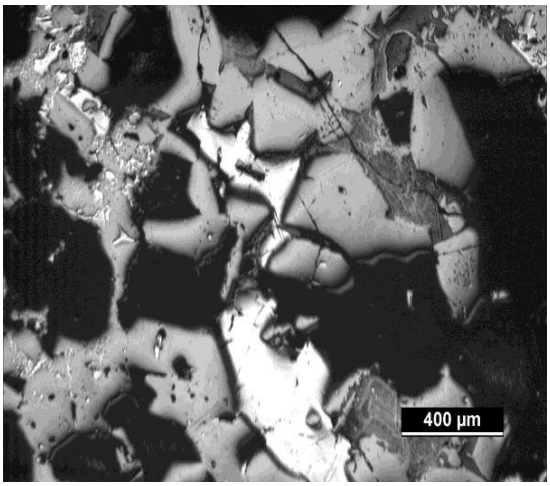

Figure 4.54 Sample No.106's micro picture

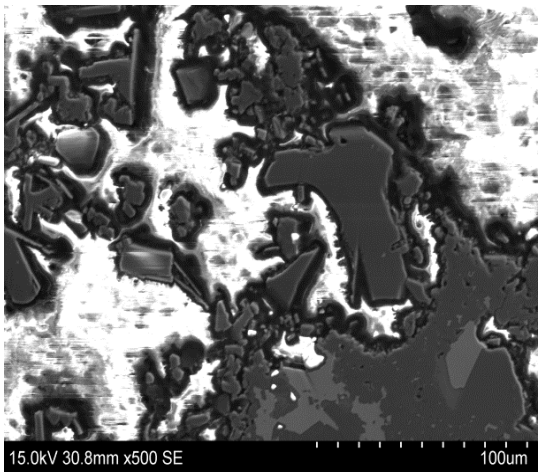

Figure 4.55 SEM image at 500x magnification

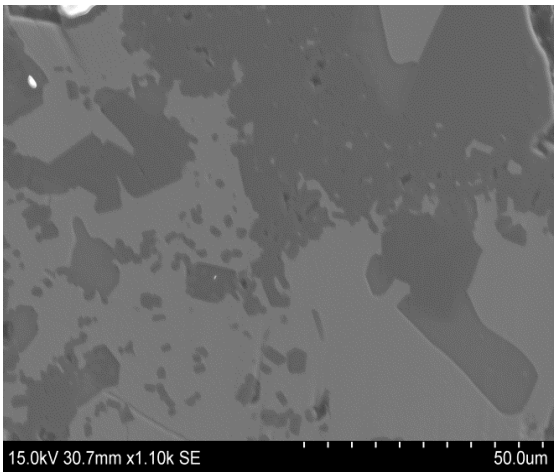

Figure 4.56 SEM image at 1100x magnification

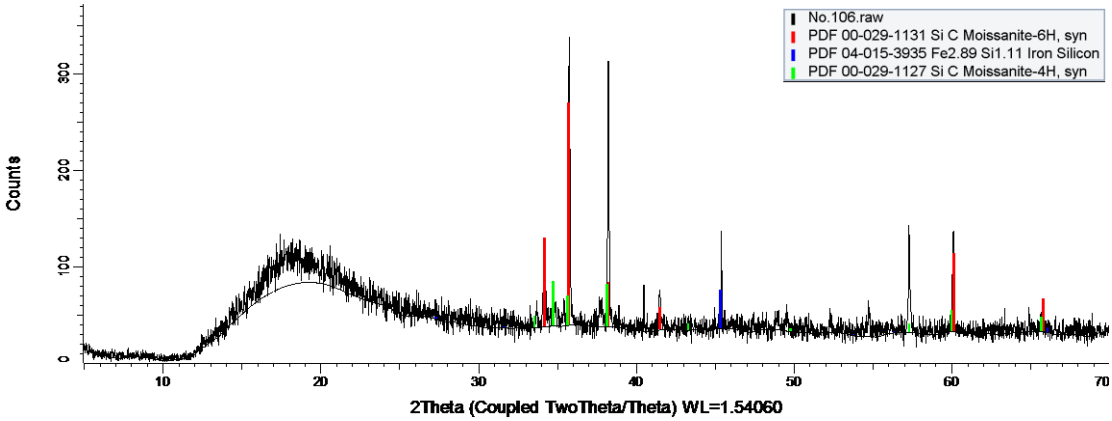

Figure 4.57 Sample No.106's XRD graph

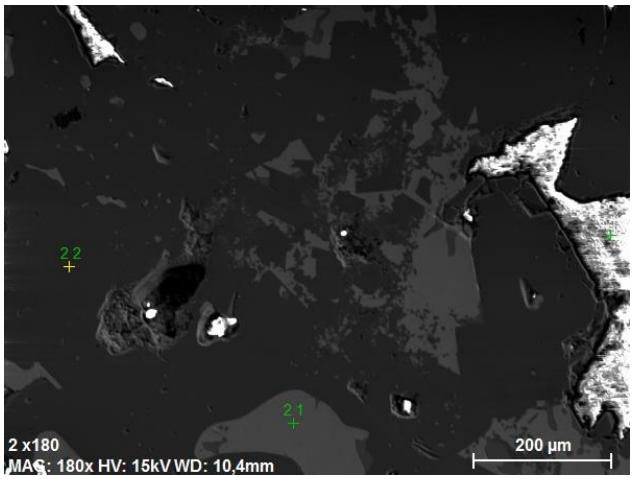

Figure 4.58 EDS image at 180x magnification

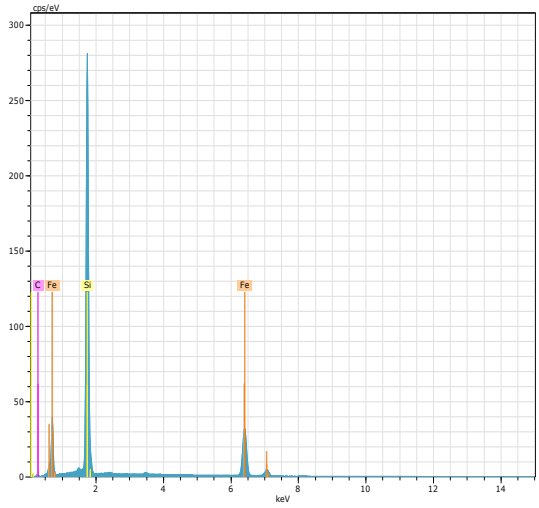

Figure 4.59 EDS graph for point 2 1

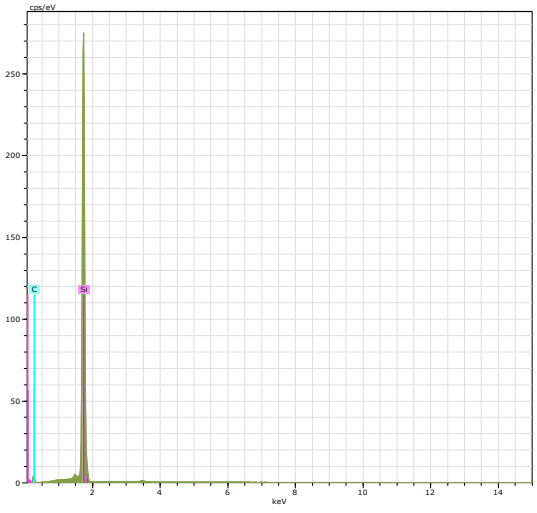

Figure 4.60 EDS graph for point 2 2

Table 4.12 EDS analysis data for point 2 1

El	AN	Series	unn. C [wt.%]	norm. C [wt.%]	Atom. C [at.%]	Error (1 Sigma) [wt.%]
C	6	K-series	2,29	2,36	7,04	0,46
Si	14	K-series	46,37	47,78	60,97	1,95
Fe	26	K-series	48,38	49,85	31,99	1,44
		Total:	97,05	100,00	100,00	

Table 4.13 EDS analysis data for point 2 2

El	AN	Series	unn. C [wt.%]	norm. C [wt.%]	Atom. C [at.%]	Error (1 Sigma) [wt.%]
C	6	K-series	13,65	20,54	37,67	1,84
Si	14	K-series	52,80	79,46	62,33	2,21
		Total:	66,45	100,00	100,00	

From these analysis data, sample No.106 is mainly composed by ferrosilicon (Point 2 1) and silicon carbide (Point 2 2). Because the atomic number of carbon is six, carbon percentages which were calculated from EDS analysis have a quite large error. In the XRD graph, the background at the beginning of the scanning was not stable. The main reason was that the samples were mounted in epoxy.

Below are sample No.111's location and analysis data. The sample was excavated from 20cm below electrode 3's tip.

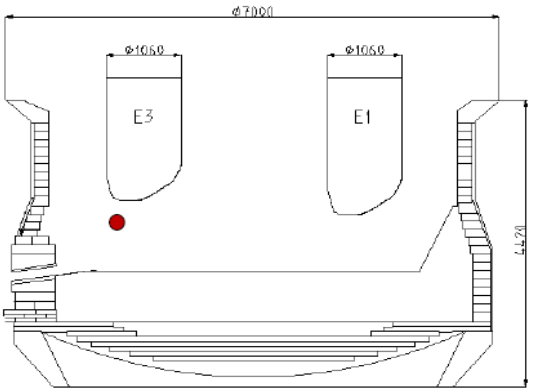

Figure 4.61 Sample No.111's location

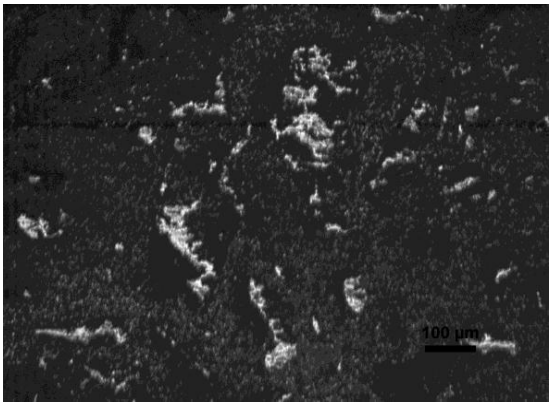

Figure 4.62 Sample No.111's micro picture

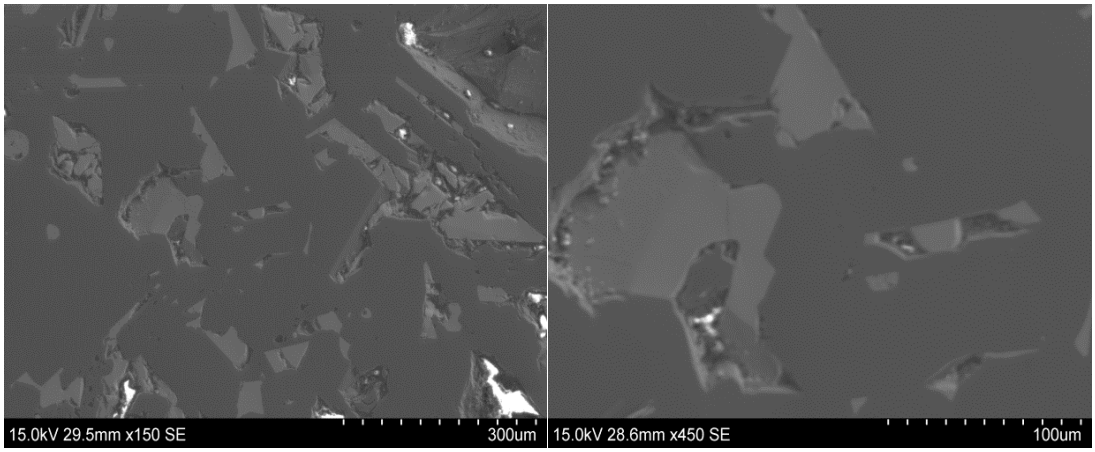

Figure 4.63 SEM image at 150x magnification Figure 4.64 SEM image at 450x magnification

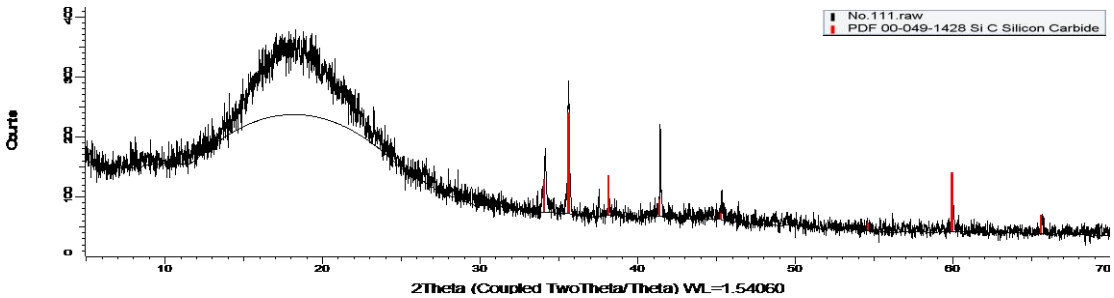

Figure 4.65 Sample No.111's XRD graph

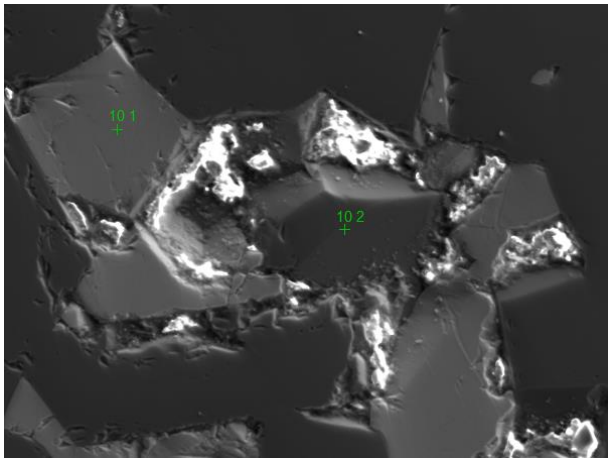

Figure 4.66 EDS image at 450x magnification

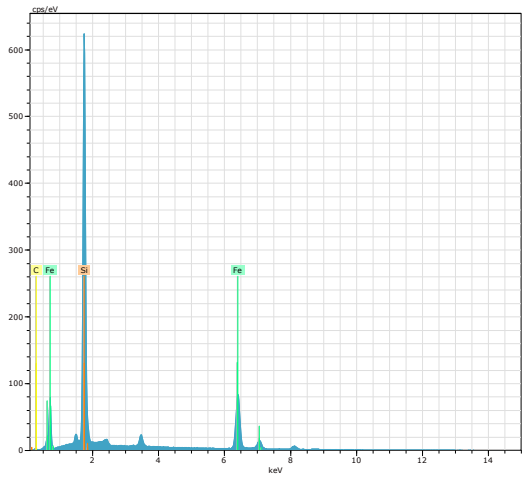

Figure 4.67 EDS graph for point 10 1

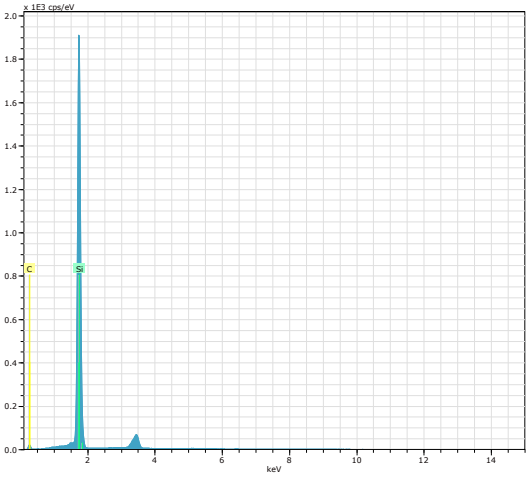

Figure 4.68 EDS graph for point 10 2

Table 4.14 EDS analysis data for point 10 1

El	AN	Series	unn. C [wt.%]	norm. C [wt.%]	Atom. C [at.%]	Error (1 Sigma) [wt.%]
C	6	K-series	0,82	1,14	3,54	0,26
Si	14	K-series	33,29	46,19	61,30	1,41
Fe	26	K-series	37,95	52,67	35,15	1,15
		Total:	72,07	100,00	100,00	

Table 4.15 EDS analysis data for point 10 2

El	AN	Series	unn. C [wt.%]	norm. C [wt.%]	Atom. C [at.%]	Error (1 Sigma) [wt.%]
C	6	K-series	12,48	16,87	32,18	1,67
Si	14	K-series	61,52	83,13	67,82	2,58
		Total:	74,00	100,00	100,00	

From these analysis data, sample No.111 is mainly composed by ferrosilicon (Point

10 1) and silicon carbide (Point 10 2). Because the atomic number of carbon is six, carbon percentages which were calculated from EDS analysis have a quite large error. In the XRD graph, the background at the beginning of the scanning was not stable. The main reason was that the samples were mounted in epoxy.

Below are sample No.113's location and analysis data. The sample was excavated 1m from both electrode 1 and electrode 3.

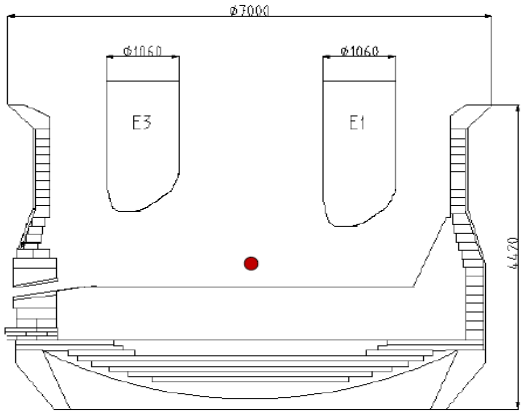

Figure 4.69 Sample No.113's location

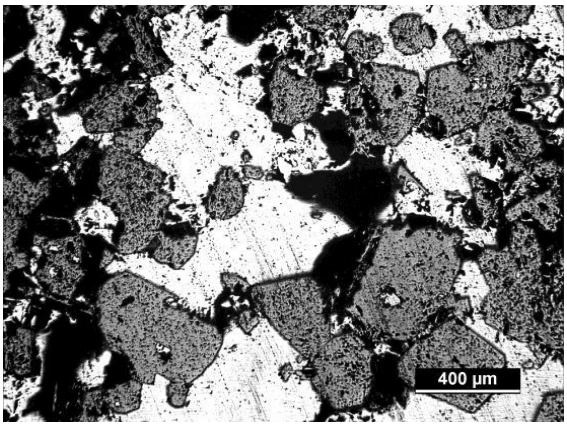

Figure 4.70 Sample No.113's micro picture

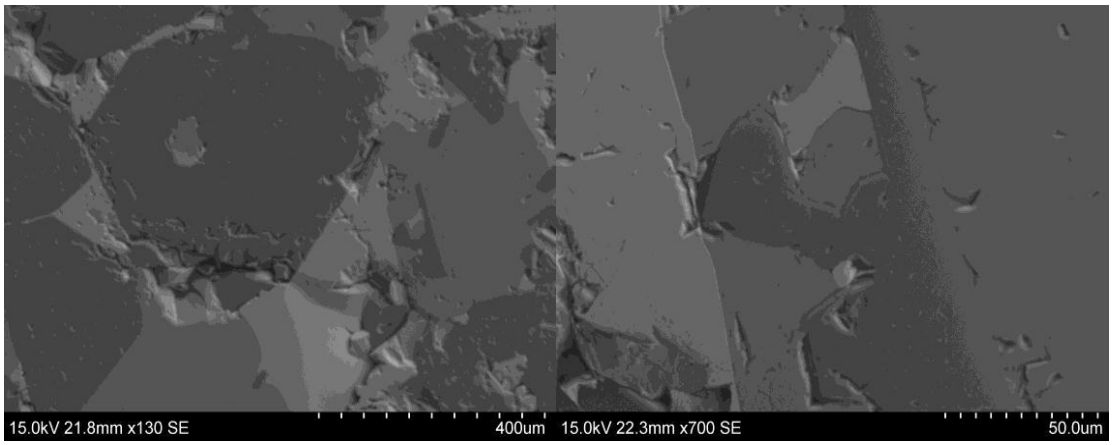

Figure 4.71 SEM image at 130x magnification Figure 4.72 SEM image at 700x magnification

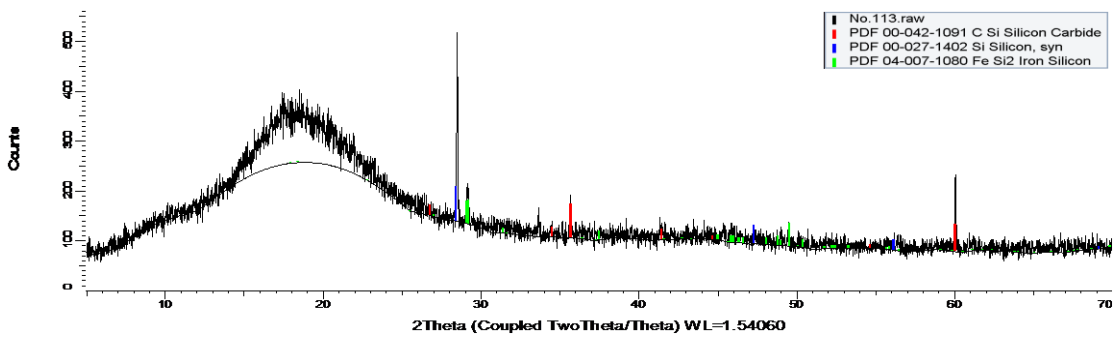

Figure 4.73 Sample No.113's XRD graph

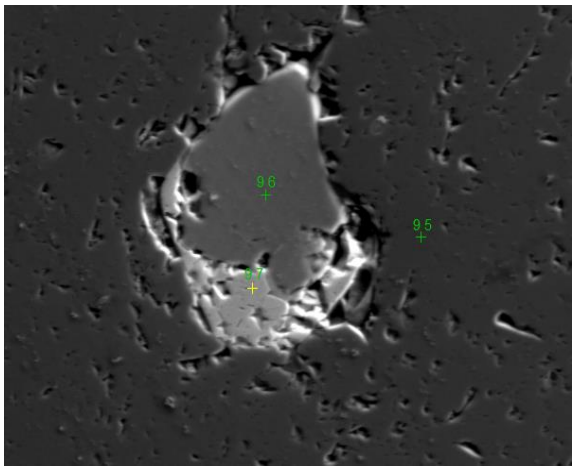

Figure 4.74 EDS image at 698x magnification

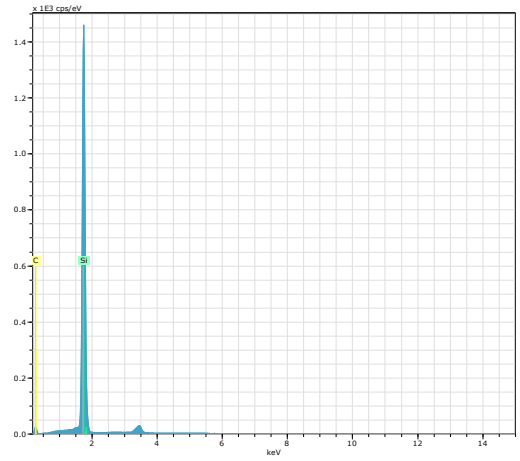

Figure 4.75 EDS graph for point 9 5

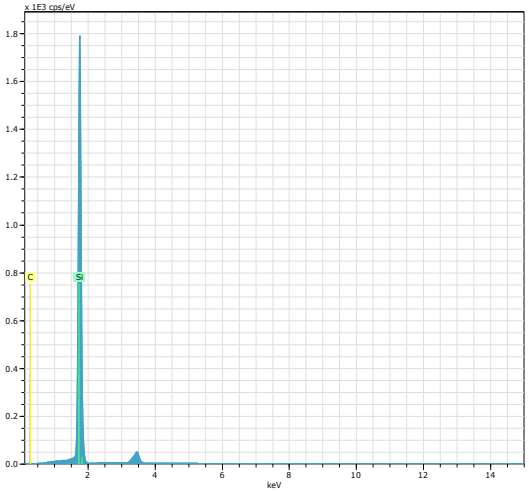

Figure 4.76 EDS graph for point 9 6

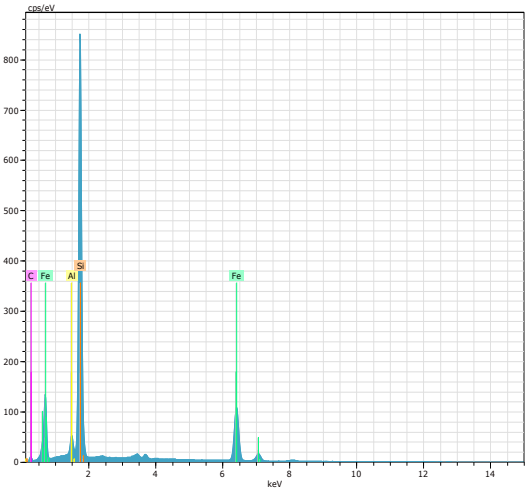

Figure 4.77 EDS graph for point 9 7

Table 4.16 EDS analysis data for point 9 5

El	AN	Series	unn. C	norm. C	Atom. C	Error (1 Sigma)
			[wt.%]	[wt.%]	[at.%]	[wt.%]
C	6	K-series	19,00	23,05	41,20	2,26
Si	14	K-series	63,42	76,95	58,80	2,65
		Total:	82,42	100,00	100,00	

Table 4.17 EDS analysis data for point 9 6

El	AN	Series	unn. C	norm. C	Atom. C	Error (1 Sigma)
			[wt.%]	[wt.%]	[at.%]	[wt.%]
C	6	K-series	4,95	5,74	12,47	0,72
Si	14	K-series	81,27	94,26	87,53	3,39
		Total:	86,22	100,00	100,00	

Table 4.18 EDS analysis data for point 9 7

El	AN	Series	unn. C	norm. C	Atom. C	Error (1 Sigma)
			[wt.%]	[wt.%]	[at.%]	[wt.%]
C	6	K-series	5,00	5,79	16,03	0,69
Si	14	K-series	39,00	45,13	53,43	1,64
Fe	26	K-series	40,62	47,01	27,99	1,21
		Total:	86,41	100,00	100,00	

From these analysis data, sample No.113 is mainly composed by silicon carbide (Point 9 5), silicon (Point 9 6) and ferrosilicon (Point 9 7). Because the atomic number of carbon is six, carbon percentages which were calculated from EDS analysis have a quite large error. In the XRD graph, the background at the beginning of the scanning was not stable. The main reason was that the samples were mounted in epoxy.

5 Discussion

From the results mentioned in Chapter 4, the samples are mainly composed by Fe, Si and C three elements. Below is a ternary phase diagram of Fe-Si-C system at 25^{o}C (Figure 5.1). The ternary phase diagram was made by FactSage 5.3 with the compound data base FACT53[8]. There is no free carbon in this ternary phase diagram when silicon percentage is higher than 50 atomic-percent. And silicon carbide was only appeared when silicon percentage is higher than 50 atomic-percent.

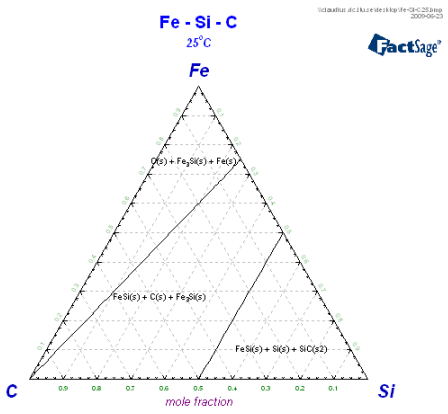

Figure 5.1 A ternary phase diagram of Fe-Si-C system at 25^{o}C[8]

Because the atomic number of carbon is six, carbon percentages which were calculated from EDS analysis have a quite large error. In the XRD graph, the background at the beginning of the scanning was not stable. The main reason was that the samples were mounted in epoxy. EPMA analysis was done in order to get more accurate data and compare the compositions of each element. As mentioned before, the samples for EPMA analysis was carbon-coated in this work. In EPMA mapping, generally the different phases can be determined by different colour. If one phase has heavier atomic weight, then the phase has lighter colour. So in this project, the phase which has the lightest colour is the ferrosilicon phase. On the contrary, the phase which has the darkest colour is the silicon carbide phase. Silicon phase's colour is between them.

This is the EPMA mapping of sample No.15 (Figure 5.2).

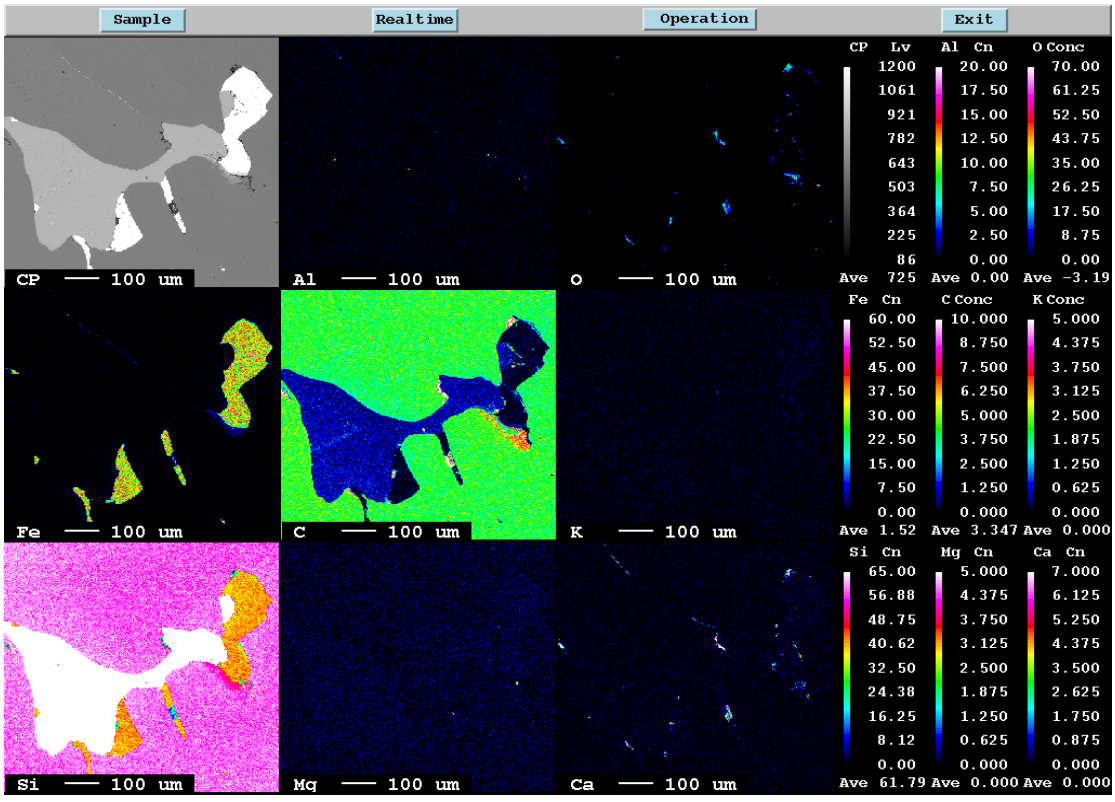

Figure 5.2 The EPMA mapping for sample No.15

In Figure 5.2, silicon, ferrosilicon and silicon carbide phases with some small area of slag phase were found. Here is a data for atomic percentage of each element in different phases (Table 5.1). The points 37-39 were in ferrosilicon phases and the

points 40-42 were in silicon phases.

Table 5.1 EPMA analysis data for sample No.15 (at%)

No.	Si	Al	Fe	C	Ca	Total	Comment
37	63.8911	0.0018	26.307	9.8001	0	100	8.1
38	64.1156	0.0247	26.4077	9.4519	0	99.9999	8.2
39	63.5707	0.0001	26.4637	9.9655	0	100	8.3
40	87.7347	0	0.1115	12.1538	0	100	8.4
41	87.6222	0	0.0126	12.3652	0	100	8.5
42	87.6281	0	0.0075	12.3643	0	99.9999	8.6

Table 5.2 Average content of each element in different phases (at%)

Phase	Si	Al	Fe	C	Ca	Total
FeSi	63.86	0.03	26.39	9.74	0	100.02
Si	87.66	0	0.04	12.29	0	99.99

In both silicon phase and ferrosilicon phase, the carbon percentage was lower when silicon percentage was higher. In this sample, the metal phase was surrounded by silicon carbide phase.

This is another EPMA mapping of sample No.75 (Figure 5.3).

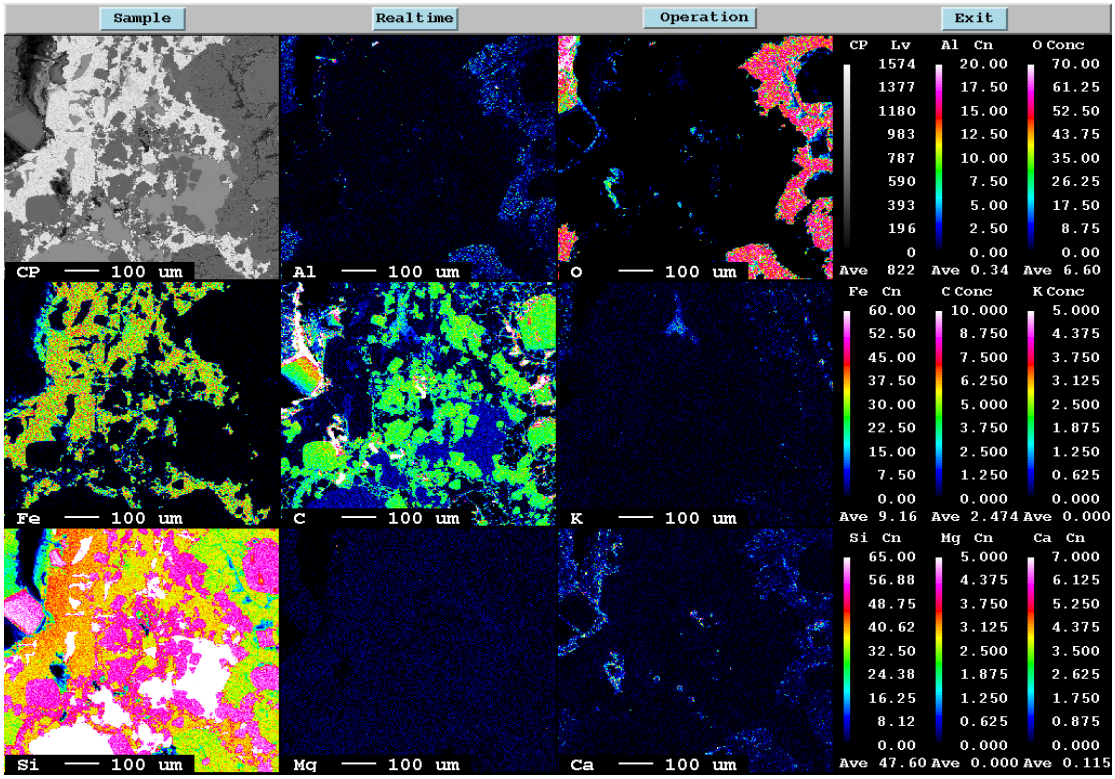

Figure 5.3 The EPMA mapping for sample No.75

From the Figure 5.3, this sample has silicon, ferrosilicon, silicon carbide and slag four different phases. Below is a data for atomic percentage of each element in different phases (Table 5.3). The points 17-20 were in ferrosilicon phases and the points 21-24 were in silicon phases.

Table 5.3 EPMA analysis data for sample No.75 (at%)

No.	Si	Al	Fe	C	Ca	Total	Comment
17	65.1514	0	25.3703	9.4784	0	100	4.1
18	64.4534	0.0246	25.7056	9.8164	0	100	4.2
19	62.9286	0.0219	26.8794	10.1701	0	100	4.3
20	62.8985	0.0267	26.9522	10.1226	0	100	4.4
21	86.528	0	0.0872	13.3848	0	100	4.5
22	87.0578	0.0007	0.0252	12.9164	0	100	4.6
23	87.6763	0	0.0424	12.2813	0	100	4.7
24	88.0703	0	0.0085	11.9212	0	100	4.8

Table 5.4 Average content of each element in different phases (at%)

Phase	Si	Al	Fe	C	Ca	Total
FeSi	63.86	0.02	26.23	9.90	0	100.01
Si	87.33	0	0.04	12.63	0	100

In both silicon phase and ferrosilicon phase, the carbon percentage was lower when silicon percentage was higher. And this data is really similar as the data from sample No.15. One was excavated from furnace top and the other one was excavated from 15cm below electrode 2’s tip. The two samples were from absolutely different location but had similar element composition in silicon and ferrosilicon phases. One more difference, sample NO.75 has a big area of slag phase.

This is EPMA mapping of sample No.82 (Figure 5.4).

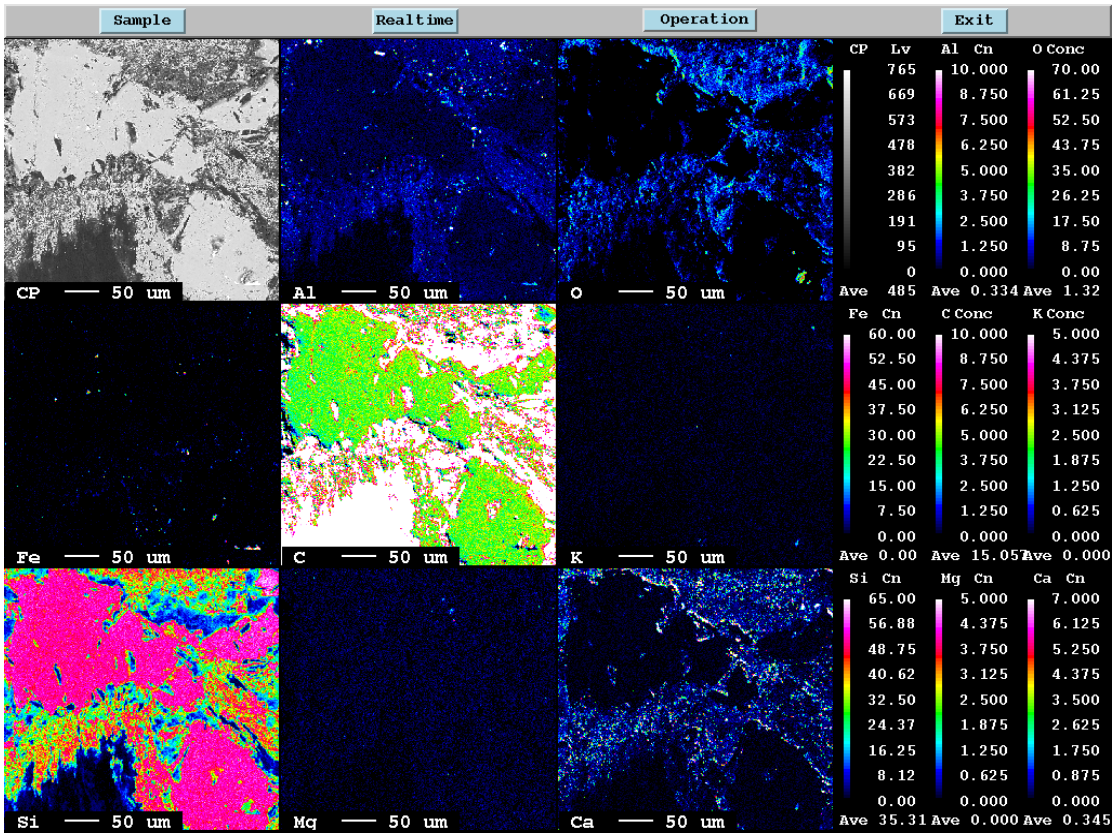

Figure 5.4 The EPMA mapping for sample No.82

This sample is mainly silicon carbide. The three points 34-36 were in silicon carbide phase. Below is a data for atomic percentage of each element in different phases (Table 5.5).

Table 5.5 EPMA analysis data for sample No.82 (at%)

No.	Si	Al	Fe	C	Ca	Total	Comment
34	46.5673	0.1561	0.0182	53.2569	0.0015	100	7.1
35	46.7989	0.0964	0.0032	53.1014	0	100	7.2
36	46.2884	0.1169	0.0041	53.5813	0.0093	100	7.3

Table 5.6 Average content of each element in different phases (at%)

Phase	Si	Al	Fe	C	Ca	Total
SiC	46.55	0.12	0.01	53.31	0	99.99

In the silicon carbide phase, the atomic ratio of silicon and carbon should be 1:1. In this data, the carbon atomic percentage is a little higher than silicon atomic percentage because this sample was carbon-coated so that it has some additional carbon.

This is the mapping of sample No.48 (Figure 5.5).

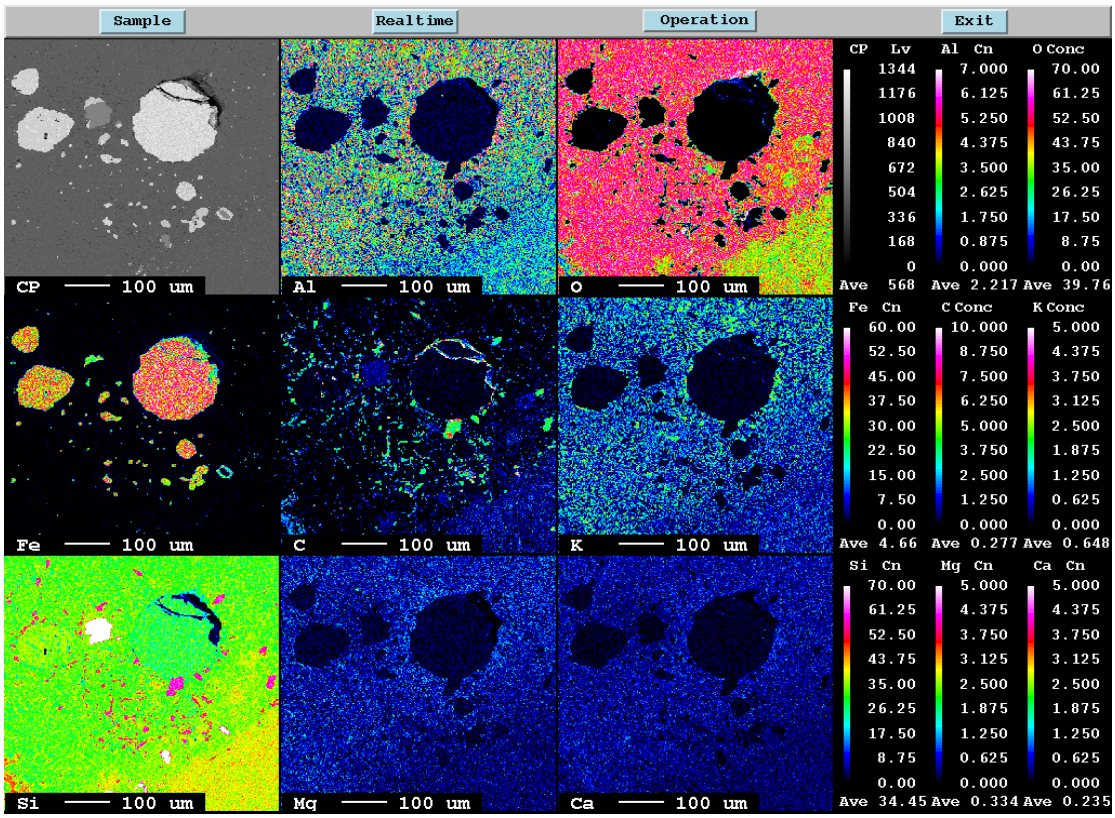

Figure 5.5 The EPMA mapping for sample No.48

In Figure 5.5, ferrosilicon and slag phases with some small dots of silicon phase were found. Here is a data for atomic percentage of each element in different phases (Table 5.7). The points 49-54 were in ferrosilicon phases.

Table 5.7 EPMA analysis data for sample No.48 (at%)

No.	Si	Al	Fe	C	Ca	Total	Comment
49	50.8544	0	36.3413	12.8043	0	100	5.1
50	51.2147	0.0018	35.8601	12.9234	0	100	5.2
51	48.4835	0	38.7978	12.7186	0	99.9999	5.3
52	54.9397	0.0522	31.4911	13.5171	0	100	5.4
53	54.2837	0.0178	32.924	12.7744	0	99.9999	5.5
54	51.1182	0.0741	35.2782	13.5294	0	99.9999	5.6

Table 5.8 Average content of each element in different phases (at%)

Phase	Si	Al	Fe	C	Ca	Total
FeSi	51.82	0.02	35.12	13.04	0	100

From Table 5.7, the iron percentage was lower when silicon percentage was higher in ferrosilicon phase. The atomic percentage of carbon has no obvious trend. It means

that the different Fe_xSi_y compounds can be formed in ferrosilicon furnace. In this sample's location, some small silicon carbide particles are found on the mapping.

Below is the EPMA mapping of sample No.106 (Figure 5.6).

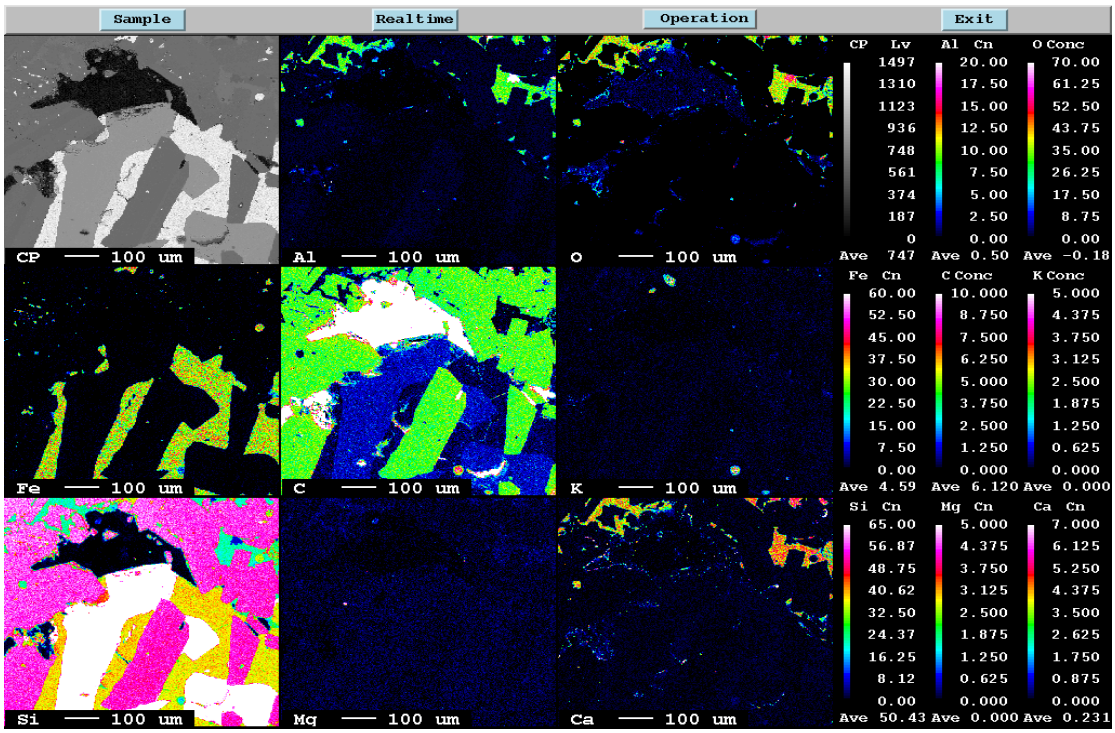

Figure 5.6 The EPMA mapping for sample No.106

From the Figure 5.6, this sample has silicon, ferrosilicon, silicon carbide and slag four different phases. Below is a data for atomic percentage of each element in different phases (Table 5.9). The points 9-12 were in ferrosilicon phases and the points 13-16 were in silicon phases.

Table 5.9 EPMA analysis data for sample No.106 (at%)

No.	Si	Al	Fe	C	Ca	Total	Comment
9	60.8566	0.0342	24.8245	14.2847	0	100	2.1
10	64.5761	0	24.9265	10.4975	0	100	2.2
11	56.0762	0.0323	24.1603	19.7311	0	100	2.3
12	58.0197	0.0354	22.4791	19.4658	0	100	2.4
13	85.8333	0.0054	0.0251	14.1362	0	100	2.5
14	85.5312	0	0.0309	14.4379	0	100	2.6
15	85.3298	0	0.081	14.589	0.0001	100	2.7
16	86.4627	0	0.124	13.4106	0.0027	100	2.8

Table 5.10 Average content of each element in different phases (at%)

Phase	Si	Al	Fe	C	Ca	Total
FeSi	59.88	0.03	24.10	15.99	0	100
Si	85.79	0	0.07	14.14	0	100

In both silicon phase and ferrosilicon phase, the carbon percentage was lower when silicon percentage was higher. In this sample, the metal phase was surrounded by silicon carbide phase.

This is another EPMA mapping of sample No.113 (Figure 5.7).

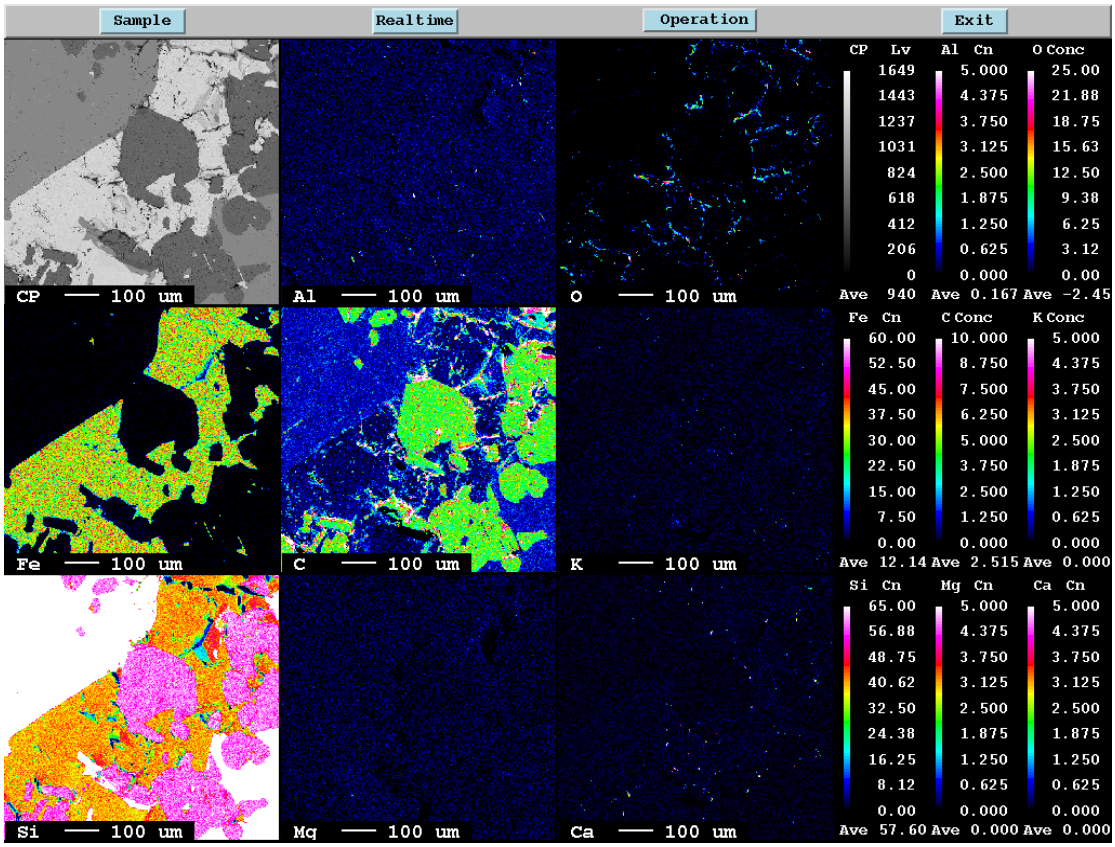

Figure 5.7 The EPMA mapping for sample No.113

From the Figure 5.5, silicon, ferrosilicon and silicon carbide phases with some small area of slag phase were found. Here is a data for atomic percentage of each element in different phases (Table 5.11). The points 43-45 were in ferrosilicon phases and the points 46-48 were in silicon phases.

Table 5.11 EPMA analysis data for sample No.113 (at%)

No.	Si	Al	Fe	C	Ca	Total	Comment
43	64.1334	0.0057	26.5253	9.3356	0	100	9.1
44	65.9511	0	27.4979	6.551	0	100	9.2
45	64.3343	0.0181	26.5192	9.1284	0	100	9.3
46	91.6105	0	0	8.3895	0	100	9.4
47	89.3816	0.006	0	10.6124	0	100	9.5
48	87.342	0	0	12.658	0	100	9.6

Table 5.12 Average content of each element in different phases (at%)

Phase	Si	Al	Fe	C	Ca	Total
FeSi	64.81	0	26.85	8.34	0	100
Si	89.44	0	0	10.55	0	99.99

In both silicon phase and ferrosilicon phase, the carbon percentage was lower when silicon percentage was higher. The sample was excavated from the bottom of the furnace both 1m from electrode 1 and electrode 3. The silicon atomic percentage in this sample is higher than any other samples from any other furnace location and the carbon atomic percentage is lower than others. We can conjecture that the furnace in this area has higher silicon percentage and lower carbon percentage in this area.

From these EPMA analyses, the Figure 5.8 shows the relationship of silicon and carbon in silicon phase in order to compare different samples more clearly. The five points are the silicon phases in each sample which are excavated from different locations. In this figure, the atomic percentages of silicon and carbon go to opposite way in silicon phase. The sample No.106 which was excavated 40cm from the charge and 35cm from the electrode 3 has the lowest silicon content and the highest carbon content. And the sample NO.113 which was excavated both 1m from electrode and 55cm below electrode 3’s tip has the highest silicon content and the lowest carbon content.

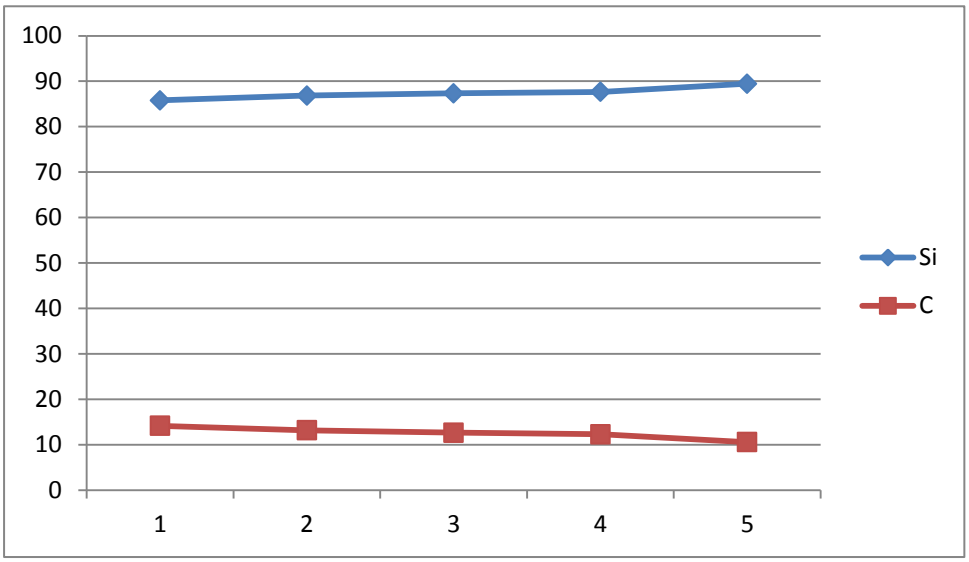

Figure 5.8 the content of Si and C in silicon phases (at%)

Below is the Figure 5.9 which shows the interaction and change between Si, C and Fe. The nine points are the ferrosilicon phases in each sample which are excavated from different locations. In this figure, iron content decreases with the increasing of silicon. In ferrosilicon furnace, it means that several different Fe_xSi_y can be formed. However, carbon content does not have an obvious trend in different ferrosilicon phases. One more interesting thing is that sample NO.106 (point five in this figure) also has the highest carbon content in ferrosilicon phase.

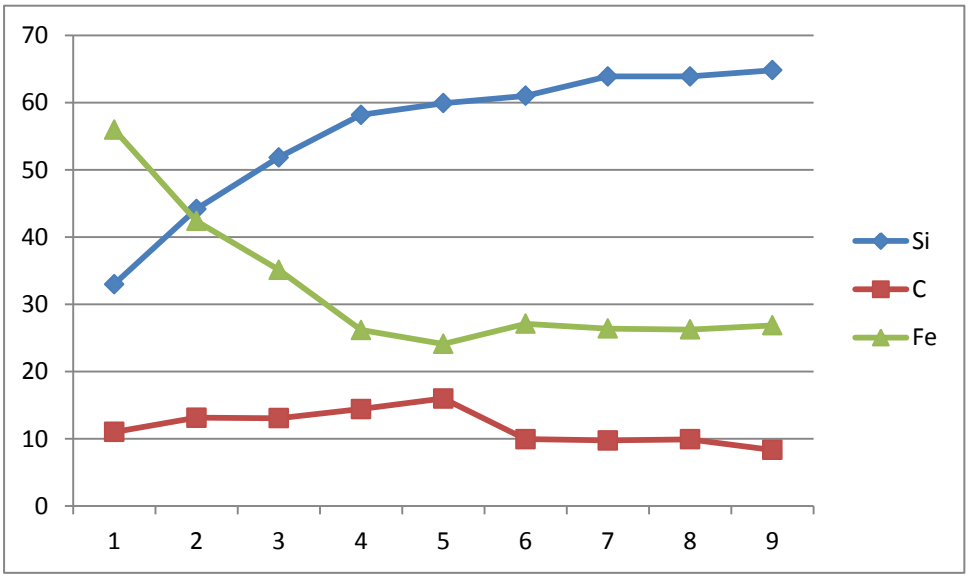

Figure 5.9 the content of Si, C and Fe in ferrosilicon phases (at%)

6 Conclusions

The carbon content in different phases and different samples has been analysed in Chapter 5. From the discussion, I get several conclusions.

First, the carbon content decreases with the increasing of silicon content in silicon phases.

Second, the carbon content has no obvious trend in ferrosilicon phases.

Third, the carbon element can be formed as silicon carbide in all locations in ferrosilicon furnace.

Fourth, the carbon content inside the silicon and ferrosilicon phases in the location where is near the outer wall is higher than elsewhere. From the analysis, most of the silicon carbide phases are formed as big particles in the samples. However, silicon carbide phase is formed as small particles in this location.

Fifth, silicon and iron can be formed as a variety of different ferrosilicon compounds in ferrosilicon furnace.

7 Challenges and Future Works

7.1 Challenges

There were several challenges during this work. These samples were from industry furnace, so have a lot of holes on the surface or inside. They were also composed of some amount of SiC resulting samples were extremely hard. Because of lots of holes and the hardness, they were too difficult to polish until surface particle diameter was 1 μm. In addition, most of samples were not good electric conductor causing some pictures from electron microscopy were not in good quality.

Carbon’s atomic number is six, so it causes large deviation during EDS analysis. The samples for EPMA analysis were carbon-coated so that the accurate carbon composition can not be known.

7.2 Future Works

One of good methods for carbon analysis needs carbon standard samples as a reference to compare already prepared samples. Using this method, one thing is necessarily to be determined that all conditions for samples preparation are in the same situation.

And analyzing more samples should be done in order to find carbon solubility trend in silicon and ferrosilicon phases.

References

1. Schei, A., J.K. Tuset, and H. Tveit, *Production of High Silicon Alloys*. 1998, Trondheim: Tapir.

2. Myrvågnes, V., *Analyses and Characterization of Fossil Carbonaceous Materials for Silicon Production*, 2008, NTNU: Trondheim.

3. Andersson, M., *Reaction Mechanisms in the Ferrosilicon Production Process*, in *Department of Chemical Engineering and Geosciences*2009, LTU.

4. Valderhaug, A., *Modelling and control of submerged-arc ferrosilicon furnaces*, in *Department of Engineering Cybernetics*1992, Norwegian Institute of Technology: Trondheim.

5. Levine D.G, S.R.H.a.S.B.G., *Understanding the chemistry and physics of coal structure.* 1982. **79**.

6. W.A, D., *An introduction to the rock-forming minarals.* 1992.

7. Can, A., *DENSIFICATION, MICROSTRUCTURE AND PROPERTIES OF LIQUID-PHASE SINTERED SILICON CARBIDE MATERIALS*, 2004, University of the Witwatersrand.

8. 5.3, F., *Compound database FACT53*.

9. Aasly, K., *Properties and behaviour of quartz for silicon production.*, in *Department of Geology and Mineral resourses Engineering*2008, NTNU: Trondheim.

10. G. Tranell, M.A., E. Ringdalen, O. Ostrovski, J. J.Steinmo, *Reaction Zones in a FeSi75 Furnace - Results from an Industrial Excavation.* INFACON 12th, 2010. **2**.

11. Utsunomiya, S. and R.C. Ewing, *Application of high-angle annular dark field scanning transmission electron microscopy, scanning transmission electron*

microscopy-energy dispersive X-ray spectrometry, and energy-filtered transmission electron microscopy to the characterization of nanoparticles in the environment. Environmental science & technology, 2003. **37**(4): p. 786-791.

12. GmbH, H.H.-T.E. *Analytical Variable Pressure FE-SEM SU6600*. Available from: http://www.hht-eu.com/cms/13987.html.

13. Reed, S.J.B., *Electron microprobe analysis.* Electron Microprobe Analysis, by SJB Reed, Cambridge, UK: Cambridge University Press, 1997, 1997. **1**.

14. JEOL. *JEOL JXA-8500F Electron Probe Micro analyzer (EPMA)*. 2011; Available from: http://www.jeol.se/.